TIME-DOMAIN SIMULATION OF SEMICODUCTOR LASER

TIME-DOMAIN SIMULATION
OF
SEMICONDUCTOR LASER
IN FIBER-OPTIC COMMUNICATION SYSTEMS

By

JIANG ZHU, B.ENG.

A Thesis

Submitted to the School of Graduate Studies

in Partial Fulfillment of the Requirements

for the Degree

Master of Applied Science

McMaster University

MASTER OF APPLIED SCIENCE (2003) McMaster University

(Electrical and Computer Engineer) Hamilton, Ontario

TITLE: Time-Domain Simulation of Semiconductor Laser in Fiber-optic Communication Systems

AUTHOR: Jiang Zhu. B.ENG. (Wuhan University of Technology)

SUPERVISOR: Dr. Wei-ping Huang

Co-SUPERVISOR: Dr. Xun Li

NUMBER OF PAGES: v, 73

ABSTRACT

As the light source, semiconductor laser diodes play an important role in the fiber-optic communication systems. The main function of a laser diode is to convert signals from the electrical domain to the optical carriers so that they can be transmitted through an optical fiber. Modeling and simulation of directly modulated laser diodes are necessary for understanding and prediction of their performance in fiber-optical communication links. The alternatives based on a comprehensive experimental evaluation are normally costly and time consuming. This is particularly true for systems running at high bit-rate such as the 10Gb/s transmission systems that are used in tele and data communication applications.

This thesis presents a modeling and simulation study for directly modulated laser diodes for high-speed fiber-optical communication systems. The work is based on the conventional rate equation model used as the governing equation for the simulation of the behavior of semiconductor lasers. In modeling of the system performance, each device is treated as a symbolic node that takes input signal and generates output signal all in time domain. For the semiconductor lasers, the original signals in electrical domain are taken as the input while the modulated lights in optical domain are as the output. The rate equations then link the output to the input. For any given time domain signal input, the modulated light (power and wavelength) as the output is calculated through the solutions of the rate equations.

In seeking for the solution to the rate equations, we utilized a numerical approach to solve the rate equations which are a system of coupled nonlinear ordinary differential equations where analytical solution does not generally exist. In this work, a comprehensive study on the behavior of semiconductor lasers has been performed through static and dynamic analyses of the rate equations. The noise characteristic is also examined as it may become a major concern in some applications for the noise of the directly modulated laser transmitter may cause degradation to the signals and therefore lead to system penalty.

Further, the numerical models and simulators developed for semiconductor lasers are incorporated into a general simulation platform on which similar models and simulators for other optoelectronic and optical components are connected to form a system-level simulator for point-to-point multiple channel fiber-optical communication links. This platform is capable of handling different system configurations with different component selection options. It simulates the time domain waveform in any point along the signal transmission path following a strict data-flow approach; i.e., the simulation is performed sample-by-sample on "real time" rather than frame-by-frame at "flush" mode.

Finally, the simulation results, both on the device level and on the system level, have been compared with the experimental data and the results from other models in literature and found qualitative agreement.

Acknowledgement

I would like to thank my supervisor, Dr. Wei-ping Huang, for his invaluable guidance, expert advice, and enthusiastic support throughout my master research period.

I would also like to acknowledge my co-supervisor Dr. Xun Li with much appreciation for his enlightenment and edification.

Specially, I want to thank my father Jiaxin Zhu, my mother Yefeng Yang and my sister Bin Zhu, for their understanding, support and endless love throughout my years of trying and learning.

Lastly, I would thank my friends, Tao Feng, Ke Zhang, Dr. Xinzhong Chen for their valuable discussion in my study and life, and the entire Photonics Research Group members in McMaster University for their advices and collaboration.

CONTENTS

CHAPTER 1

1 INTRODUCTION

With the invention of the low-loss optical fibers as an ideal transmission media for long-haul and high-speed communications in 1970, the development of fiber-optic communication systems and networks has gone through several technological generations and in the meanwhile made significant impact on the construction of global information infrastructure and our everyday life.

In its simplest, generic form, a basic fiber-optical communication system is shown in *Figure 1-1* , in which the system consists of an optical transmitter, an fiber optic link, and an optical receiver.

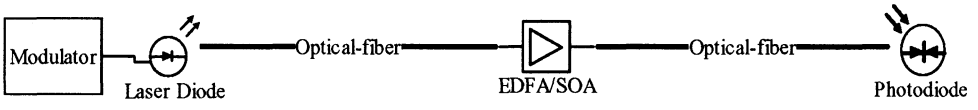

Figure 1-1 Basic sketch of optical communication system

At the heart of the optical transmitters lies the optical source, which is normally a semiconductor laser diode, either directly modulated or running at continuous state and connected with an external modulator. For the former is structurally simpler and more convenient, yet the intrinsic interplays between the electrical carriers and the optical fields in the laser diodes make the dynamic characteristics of the laser diodes under direct modulation complex in nature.

The goal of optical communication system is to transmit information using light wave from the transmitter end to the receiver end over a long stretch of optical fiber.

Normally, the semiconductor laser diode is modulated by electrical pulse, presented as a series of '1's or '0's. The output of the laser diode is a train of optical envelope pulse populated with '1's or '0's. The modulated optical signals then travel along the optical fiber. As the optical signals propagate through the optical fibers, attenuation and distortion due to the fiber loss and dispersion/nonlinearity unavoidably happen. Like other traditional communication links, amplifiers, or repeaters in optical domain are required to compensate for the corresponding transmission loss (in the case of amplifiers) or distortion (in the case of repeaters). At the receiver, the optical signals are detected by a photo-detector which converts the optical envelopes into electrical signals that are further amplified. Finally, the electrical signals are sent to a decision circuit, which determines whether '1' or '0' has been received. In reality, noises will be generated and added to the signals during signal generation, amplification, and detection. Consequently, the information is contaminated by all kinds of noises and distortions introduced by the optical components when arriving at the receiver end.

Simply speaking, the reason we use computer to simulate optical telecommunication systems instead of setting up a real hardware testing project is that, in the initial stage of the design in optical devices and systems, we can set up models in computer, not real sample products, to see the performance required without spending a large amount of experimental budget. The focus of this thesis is on the simulation of semiconductor lasers as the optical transmitter in the context of an optical telecommunication system through numerical methods. In chapter 2, we will discuss the basic features of semiconductor lasers. In chapter 3, based on the behavior of a semiconductor laser, we establish the time domain behavior models in the form of coupled ordinary differential equations. In chapter 4, we will explain in great detail how to solve these ordinary differential equations and in chapter 5 we show the numerical solutions of the laser behavior models. In chapter 6, noises are further taken into account in the simulation of semiconductor lasers. Finally, in chapter 7 we will incorporate the laser module into the system simulation package, which has been implemented as part of the thesis related work, to predict the system performance.

CHAPTER 2

2 BASIC LASER PHYSICS

This chapter reviews basic concepts and the operating mechanism of the semiconductor lasers. It is the foundation of the governing rate equations for the modeling and simulation of direct-modulated semiconductor laser diodes in this thesis.

2.1 Laser Emission Mechanism

A laser is an optical source that is capable of emitting highly intense, pure and coherent lights. In order to achieve these characteristics in a semiconductor laser, two important conditions are indispensable: (i) a gain medium that can amplify photons in the laser cavity and (ii) a feedback mechanism that form a resonator to confine the optical fields. For a semiconductor laser, the gain medium is achieved by semiconductor materials. The optical feedback is obtained by using the cleaved facets in Fabry-Perot type cavity. To get the optical gain sustainable, external pumping of electrical carriers is required for a semiconductor laser, which is implemented by using a forward-biased injection current over a $p-n$ junction.

2.2 Laser Diode Structure

A laser diode is a $p-n$ junction with an optical feedback mechanism. *Figure 2-1* shows a basic laser structure. A $p-n$ junction is formed by putting a p-type and an n-type semiconductor material together. In the active region the $p-n$ junction forms, electrons and holes combine together, thus generating light emission. Also cleaved facets make two

mirrors at each end longitudinally resulting in feedback like a cavity. Light generated travels back and forth in the cavity, and further light is amplified and purified. For successful laser operation, carrier (electrons and holes) density is extremely high at low injection current, and also light field requires remaining in the vicinity of the active region. To realize a viable lasing oscillation, double hetero-structure has proved to be a good structure in most up-to-date semiconductor lasers. From *Figure 2-2*, for a hetero-structure laser, the active layer with lower band gap is sandwiched by p-doped and n-doped semiconductor materials as cladding layers. With the structure shown is *Figure 2-2,* electrons and holes can only combine in the active layer, preventing electrons (holes) from passing into the p(n)-doped layer because of the larger band gap in cladding than in active region. Coincidently, the active layer with a smaller band gap also has a higher refractive index compared to the cladding layers with lower ones, leading to optical field confinement due to the internal reflections at the interfaces.

2.3 Optical Gain in Recombination Mechanisms

In a laser, there are three types of recombination for electrons and holes: stimulated absorption, spontaneous emission, stimulated emission. We usually use a two-level model to demonstrate this transition for the carriers. *Figure 2-3* shows that it is the three transitions that govern every fundamental process. While forward bias voltage applies, the internal built-in electrical field is reduced making the diffusion of electrons and holes in the active region further. In the active region, electrons and holes can recombine together through stimulated absorption, spontaneous emission, or stimulated emission. Under normal conditions, all materials absorb light instead of emission of light. If a photon with $h\nu$ is the same as the band gap energy $E_g = E_C - E_V$, where E_C, E_V presents the energy level of conductor band and valence band, respectively, an electron is moved from the valence band into the conductor band with absorption of the photon, leaving behind a hole in the valence band. However, at the same time, electrons in the conductor band are not yet at the steady state, some electrons drop back to the valence band again with emission of

photons. The process is called spontaneous emission in which photons emitted are in random directions with no phase correlation. Also with the stimulation of an existing photon, a new photon gets generated with the same direction, frequency, phase, and energy as the existing one, and simultaneously, an electron in the conductor band drifts back to the valence band. When the external voltage exceeds a critical value, a condition called the population inversion is achieved, in which the rate of photon generation by spontaneous emission and stimulated emission surpass that of absorption. In another words, the density of electrons in conductor band should be larger than that in valence band to get the condition satisfied. Until this moment, photons can generate more photons in laser with continuous external voltage or external pumping, thus forming positive gain or amplification in active region, i.e. optical gain.

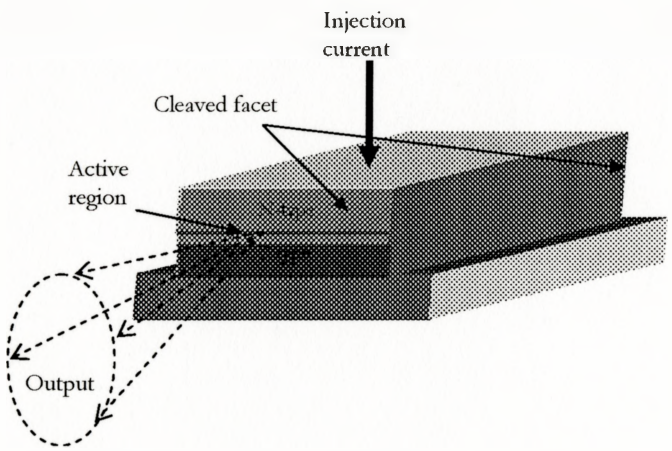

Figure 2-1 Schematic diagram of a basic double-heterostructure semiconductor laser

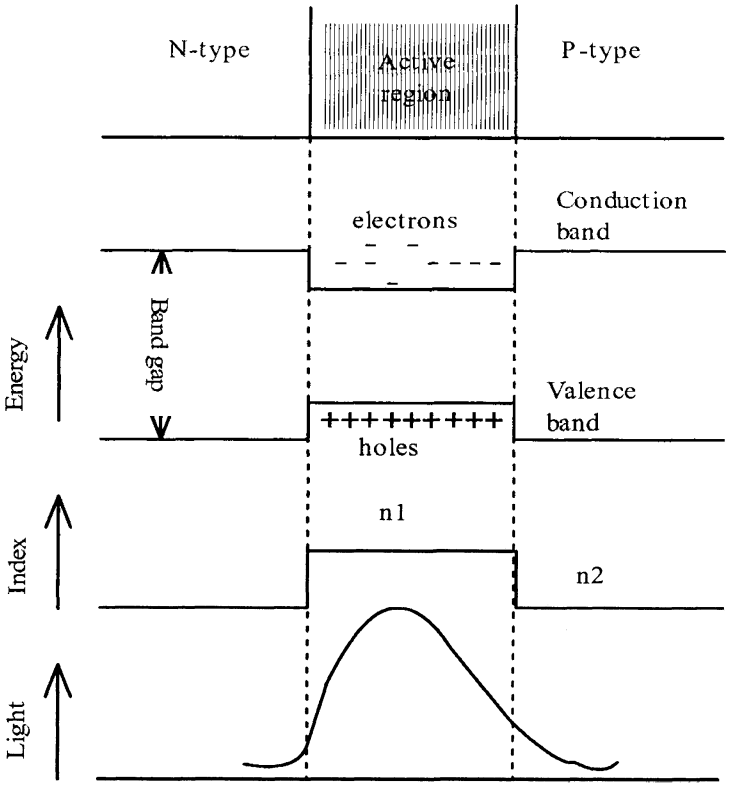

Figure 2-2 Confinements of carriers and optical modes by using double-heterostructure

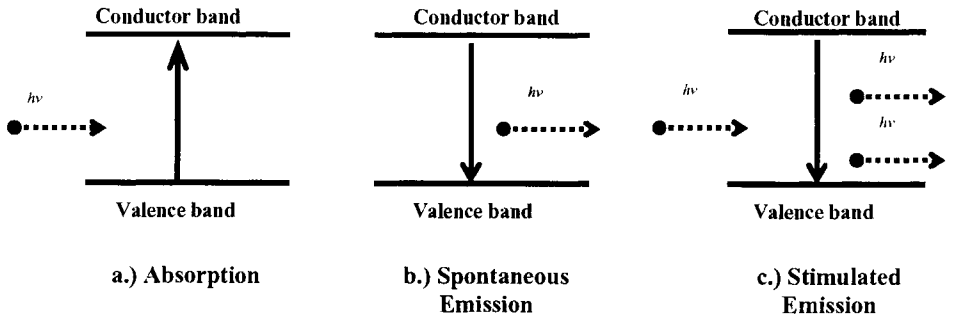

Figure 2-3 Schematic diagram of two-level system describing the transitions (a.) absorption, (b) spontaneous emission and (c) stimulated emission.

CHAPTER 3

3 RATE EQUATION MODEL

Laser dynamic characteristics can be described either by rate equations that depends on time only or by traveling wave equations that have both time and space dependences [1] [18] [21]. In system simulation, the laser is taken as a symbolic node that takes the input signal in electrical domain and converts it into a modulated light in optical domain. From this point of view, the rate equation [13] [14] based model is sufficient as we just need to link the output signal to the input signal for the given laser parameters. Noting the fact that the input, bias current, can only be connected to the output, optical power and lasing wavelength, through the carrier, we have to use three separate equations that describe the dynamics between the bias current and the carrier, the carrier and the optical power, and the carrier and the lasing wavelength, respectively.

3.1 Stimulated Emission Rate and Optical Gain

The stimulated emission is the net emission that is the difference of the carrier downward transition and upward transition triggered by the photons. According to the laser emission mechanism described in the previous chapter, the stimulated emission dominates only in the condition of population inversion. To satisfy this inversion condition, strong external injection into the active region is required. These facts suggest that the stimulated emission must be associated with both of the carriers and the photons.

The stimulated emission rate is defined as:

$$R_{st} = v_g \Gamma g_m S \quad \textit{Equation 3-1}$$

where v_g is the group velocity, Γ the confinement factor that indicates the ratio between the optical field inside the active region and the total field, S the photon number and

$$g_m = a[N - N_{tr}], \text{for Bulk material}$$
$$g_m = a \ln \frac{N}{N_{tr}}, \text{for QW material} \qquad \textit{Equation 3-2}$$

In these expressions, g_m is the peak gain for a given carrier density [13], N the carrier density, N_{tr} the transparency carrier density at which population inversion is achieved, and beyond which, optical gain is positive, a the gain coefficient.

3.2 Photon Rate Equation

The photon change rate must be equal to the total photon generation rate minus the total photon consumption rate. Noticing the fact that the total photon generation rate is the sum of the stimulated emission rate and the spontaneous emission rate, and the photons are consumed through the cavity leakage (the leaked photons form the light output) and through various absorption and scattering processes other than the inter-band absorption, we have:

$$\frac{dS}{dt} = R_{st} + K \Gamma v_g n_{sp} g_m - S / \tau_{ph}$$

or:

$$\frac{dS}{dt} = S (\Gamma v_g g_m - 1 / \tau_{ph}) + K \Gamma v_g n_{sp} g_m \qquad \textit{Equation 3-3}$$

This equation can also be obtained from the wave equations [14]. The first term on the right hand side of the photon rate equation represents the stimulated emission contribution as specified in the previous section; the second term represents the total photon consumption. These two terms are obviously proportional to the photon numbers. The third term represents the spontaneous emission contribution with K denoting the Petermann's factor [19], n_{sp} the population inversion factor given as the ratio between the spontaneous emission rate and the stimulated emission rate, τ_{ph} the photon life time defined by:

$$\frac{1}{\tau_{ph}} = v_g[\alpha_{\text{int}} + \frac{1}{2L}\ln(r_r r_f)] \quad \textit{Equation 3-4}$$

In this expression, the first term on the right hand side represents the total internal photon losses that count all the absorption and scattering processes other than the inter-band absorption with a_{int} defined as the internal loss per unit length along the wave propagation (cavity) direction. The second term represents the cavity loss that count the photon leakage from both ends of the laser with L defined as the laser cavity length, r_r and r_f the rear and the front facet reflectivity, respectively.

3.3 Phase Rate Equation

In addition to the rate equation for photon numbers, the phase rate equation can also be derived from the wave equations [14]:

$$\frac{d\phi}{dt} = \frac{1}{2}\alpha_{LEF}\,\Gamma v_g g_m \quad \textit{Equation 3-5}$$

with α_{LEF} defined the line width enhancement factor [24]. This equation is associated with the frequency chirp or the wavelength shift. When the bias current changes as function of time, the carrier also changes hence the gain follows the change according to Equation 3-2. Therefore, as the derivative of the phase in respect of the time, the lasing frequency varies with the bias current. Such parasitic modulation effect is known as the frequency chirp or wavelength shift and can readily be evaluated though the phase rate equation.

3.4 Carrier Rate Equation

Similar to the balance requirement for the photon rate equation, the carrier change rate must be equal to the total carrier generation rate minus the total carrier consumption rate. Therefore, we have:

$$\frac{dN}{dt} = \frac{I}{qV} - \frac{N}{\tau_n} - \frac{1}{V}R_{st} = \frac{I}{qV} - \frac{N}{\tau_n} - \frac{1}{V}\Gamma v_g g_m S \quad \textit{Equation 3-6}$$

The first term on the right hand side of this equation stands for the carrier generation rate from the external injection into the active region. The second term is related to the carrier consumption through the non-radiative recombination and the spontaneous emission. The last term represents the carrier consumption through the stimulated emission, which leads to a strong nonlinear coupling between the photons and the carriers. In this expression, I denotes the bias current, q the unit charge, V the volume of the active region, and τ_n the carrier lifetime.

3.5 Multimode Rate Equations

The previous equations describe the behavior of the semiconductor laser under single mode operation. However, semiconductor lasers with Fabry-Perot cavity exhibit

multiple longitudinal modes. Therefore, the above rate equation model must be expanded for multimode operations.

It is obvious that multiple photon rate and photon phase equations must be introduced to describe the behavior of each mode. As the gain spectrum is not uniform, different lasing mode will find different gain as their lasing frequencies are all different. The gain spectrum can be obtained through experiment or physics-based numerical models. In this work, a simple approximation on the gain profile is adopted; i.e., the gain is assumed to have a parabolic-like shape with its peak value given in *Equation 3-2*. Such gain profile is sketched in *Figure 3-1*.

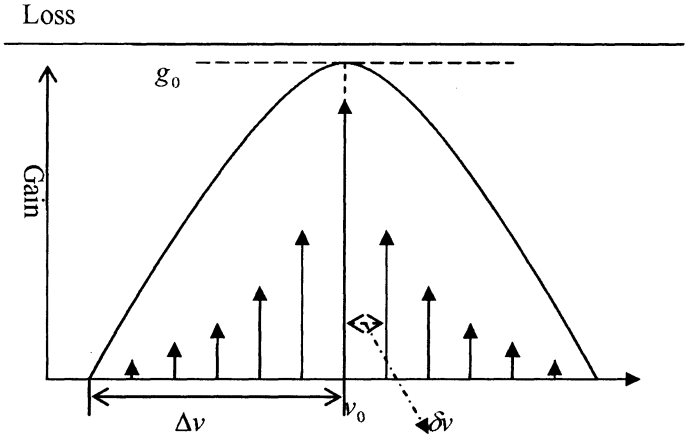

Figure 3-1 Sketch of gain profile with symmetry and parabolic assumption

By introducing a parameter known as the detuning factor D_j to count the gain depreciation when the lasing mode is set away from the gain peak position, we have:

$$D_j = 1 - \left(\frac{v_j - v_0}{\Delta v}\right)^2 \quad \textit{Equation 3-7}$$

where v_0 is the gain peak frequency, Δv the width of the gain profile at which the gain drops to zero, and v_j the frequency of the j-th lasing mode. As the lasing modes of the FP laser are equally spaced, we have:

$$v_j = v_0 + j\delta v \quad \textit{Equation 3-8}$$

where j is an integer varying from $-J$ to J, $J \cong \frac{\Delta v}{\delta v}$ and δv denotes the mode spacing determined by the FP laser cavity length through $\delta v = c/2n_g L$ with c defined as the speed of the light in free space and n_g as the group velocity.

Therefore, the optical gain for the j-th mode is give as:

$$g_{m,j} = g_m D_j = g_m[1 - (\frac{v_j - v_0}{\Delta v})^2] \quad \textit{Equation 3-9}$$

where g_m is the peak gain at frequency v_0 and is given by *Equation 3-2* .

In addition to the detuning factor, the nonlinear gain suppression should also be considered as different mode may find different suppression as different mode usually has different photon numbers. Hence the linear gain $g_{m,j}$ should be replaced by $g_{m,j}/(1+\varepsilon S_j)$, where factor $1/(1+\varepsilon S_j)$ describes the nonlinear gain suppression for different lasing modes with ε defined as the nonlinear gain suppression coefficient and S_j the photon number of the j-th mode. This effect is known as the spectral hole burning and is clearly described in [20].

Follow a similar procedure as above, we obtain the multimode rate equations:

$$\frac{dS_j(t)}{dt} = S_j(t)[\Gamma v_g g_{m,j}(t) - \frac{1}{\tau_{p,j}}] + \Gamma K v_g n_{sp} g_{m,j}(t),\ j = 1,2,...,\ M$$

$$\frac{d\phi_j(t)}{dt} = \frac{1}{2}\alpha_{LEF}\ \Gamma v_g g_{m,j}(t),\ j = 1,2,...,\ M$$

$$\frac{dN(t)}{dt} = \frac{I(t)}{qV} - \frac{N(t)}{\tau_n} - \frac{\Gamma v_g}{V}\sum_{j=1}^{M} g_{m,j}(t) S_j(t)$$

$$g_{m,j}(t) = a[N(t) - N_{tr}][1 - (j\frac{\delta v}{\Delta v})^2]/[1 + \varepsilon_j S_j(t)],\ \textit{Bulk}$$

$$g_{m,j}(t) = a \ln\frac{N(t)}{N_{tr}}[1 - (j\frac{\delta v}{\Delta v})^2]/[1 + \varepsilon_j S_j(t)],\ \textit{QW}$$

Equation 3-10

Equation 3-10 forms our final governing equations and will be used for the simulation of the semiconductor FP lasers.

CHAPTER 4

4 NUMERICAL IMPLEMENTATION

In order to obtain the laser performance, the set of coupled nonlinear ordinary differential equations extracted must be solved numerically. Different algorithms have been implemented in this chapter for the steady state and dynamic analysis, respectively.

4.1 Static and Dynamic Analysis

With laser behavior rate equations, the next step is to solve all these coupled nonlinear equations. In computer simulation, the numerical methods should be chosen appropriately to accommodate the effective results. We solve all $S_j(t), \phi_j(t), N(t)$ in time-domain, taking injection current $I(t)$ as the given initial condition and all other parameters such as laser structure parameters, system operation parameters are given.

Firstly, we should consider laser behavior in steady state, or all the derivative terms are equal to zeros ($\frac{dS}{dt} = 0; \frac{d\phi}{dt} = 0; \frac{dN}{dt} = 0$). Then use the corresponding numerical method to solve these nonlinear equations.

Secondly, for dynamic laser behavior, we will employ the outcome from the solutions in steady state as the initial guess to step into the transient algorithm, thus getting the results under dynamic conditions.

4.2 Numerical Approach for Steady State Analysis

Here we will further discuss the numerical methods [15] [16] for steady state solution and dynamic solution.

As mentioned above, we should set the derivatives of the nonlinear coupled equations equal to zeros to get the steady solutions. For analytical solution, we can directly set the values. However, it is difficult to solve coupled nonlinear equations, especially for multimode equations to get analytical solution. It is more practical to rely on numerical computations. Newton's Method with a globally convergent strategy is a way to solve root finding problems for this kind of nonlinear equations. Here we almost utilize the most sophisticated Newton's Method, since simpler Newton's method has very inefficient ability in the global convergence problems.

On input side, the first beginning point is at the transparency point where upward stimulated emission rate is equal to downward stimulated emission rate. That means that after the point there exist photons in cavity, before this point, we consider the number of photons being zero.

On output side, the data saved in files are photon powers, wavelengths for certain carrier densities in steady state, which will be used in later dynamic computation.

Channel j (related to frequency j) optical power $P_j(t)$ in [W] is given by

$$P_j(t) = h\nu_{ref} v_{g,j} \alpha_c S_j(t) \quad \textit{Equation 4-1}$$

,where h is the Plank constant in [J/s], v_{ref} is the reference frequency in [1/s], α_c is the cavity loss in [1/cm].

Channel j (related to frequency j) wavelength $\lambda_j(t)$ in [nm] is given by

$$\lambda_j(t) = \frac{\lambda_{ref}^2}{2\pi v_{g,j}}\left(\frac{d\phi_j(t)}{dt}\right) + \lambda_{ref} \quad \textit{Equation 4-2}$$

,where $\lambda_{ref} = 10^7 v_g / v_{ref}$ is the reference wavelength in [nm] and v_g is the average group velocity in [cm/s].

We will describe the detailed implementation steps of Newton's method with globally convergent strategy in the following paraphrase to get the steady state solutions.

The Implementation Steps:

1. Check if the values of S_0, N_0 at transparency point I_0 are the roots for the Non-linear functions which are the right part of ordinary differential equations. If yes, go to (5)

2. If no, make a full Newton step ΔI to check the convergence, and also check the condition $f(x_{new}) \le f(I_{old} + \alpha \nabla f \bullet (I_{new} - I_{old}))$ where $f = \frac{1}{2}\vec{F} \bullet \vec{F}$, $\vec{F}$ denoting the entire vector of functions, making the functions based on the step decrease sufficiently.

   If the convergence on ΔI satisfied, go to (4).

3. If the above condition satisfied, calculate new I and f, and check the convergence either on function value or on ΔI, if one of either satisfied, go to (4).

   If the step ΔI is not acceptable, try to adjust the λ, which comes from $I_{new} = I_{old} + \lambda \Delta I, 0 < \lambda \leq 1$ (using the line searching and backtracking to get the condition meet.)

4. Calculate and output S, N, ϕ in certain current stage

Below *Figure 4-1* shows the schematic flow diagram of Newton's method in implementation of laser simulation.

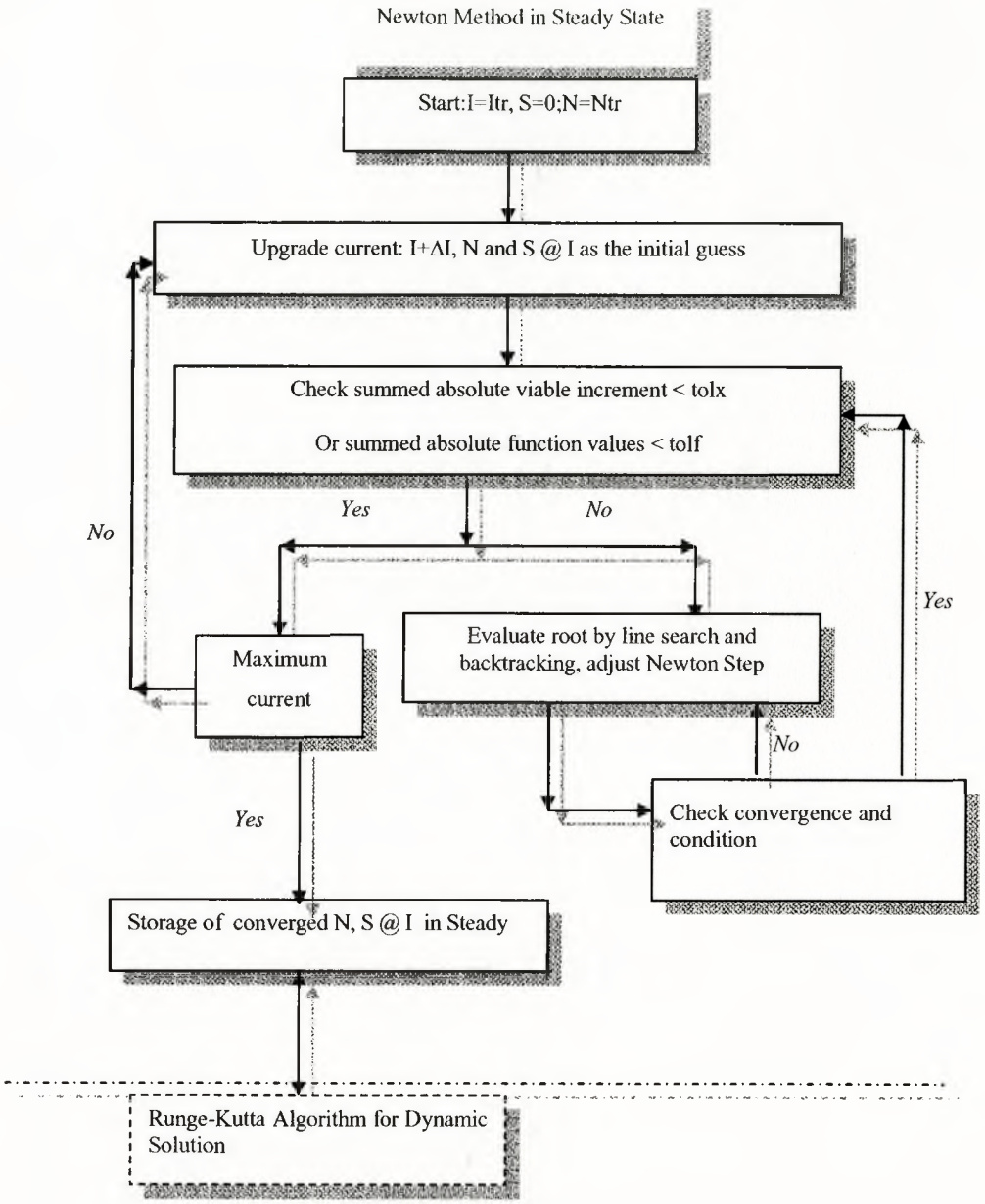

Figure 4-1 Data flow of steady state solution

4.3 Numerical Approach for Dynamic Analysis

To simulate laser operating under transient state, we have to use another strategy to solve these nonlinear ordinary equations. For solving this kind of ODEs, we normally already have these values at starting points ready. Therefore, we can choose Runge-Kutta methods to solve the initial value problems. Both fourth-order Runge-Kutta with fixed step size and fifth-order Runge-Kutta with adaptive step size control are implemented in our simulation package. Also for the precision in our simulation, fourth-order Runge-Kutta are very capable with the simulation, and get the same reasonable results as the fifth-order Runge-Kutta with adaptive size control mechanism. With the principle of simplicity and efficiency, we just choose fourth-order Runge-Kutta as the code block appearing in later chapters. Also we still provide the diagrams and descriptions of the Runge-kutta with both fixed step and adaptive step size control in this chapter, in case for high precision demand in the later future research purpose.

On input side, the initial starting values S_0, N_0 are obtained from the tabulation calculated from Newton's Method given certain injection current stages directly from bit stream or output of external modulator.

On output side, the data of the optical powers and wavelengths save in file and deliver to next simulation block such as optical-fiber simulation block.

The fourth-order Runge-Kutta with fixed step implementation steps are below:

1. Look up the values of S_0, N_0 in the tabulation generated from steady state solution, corresponding to the output current from the previous block. If found in the tabulation, go to (3)

2. If not found, to find the closest two neighbours, do linear interpolation, calculating the values of S_0, N_0.

3. Advance one fixed step h_{fixed}, using fourth-order Runge-Kutta algorithm to get the solution over the step. Return the incremented values S_{n+1}, N_{n+1}.

4. Save the calculated results from step (3) and Check if the final step reached, if not, go to (3). If yes, exit the Runge-Kutta loop.

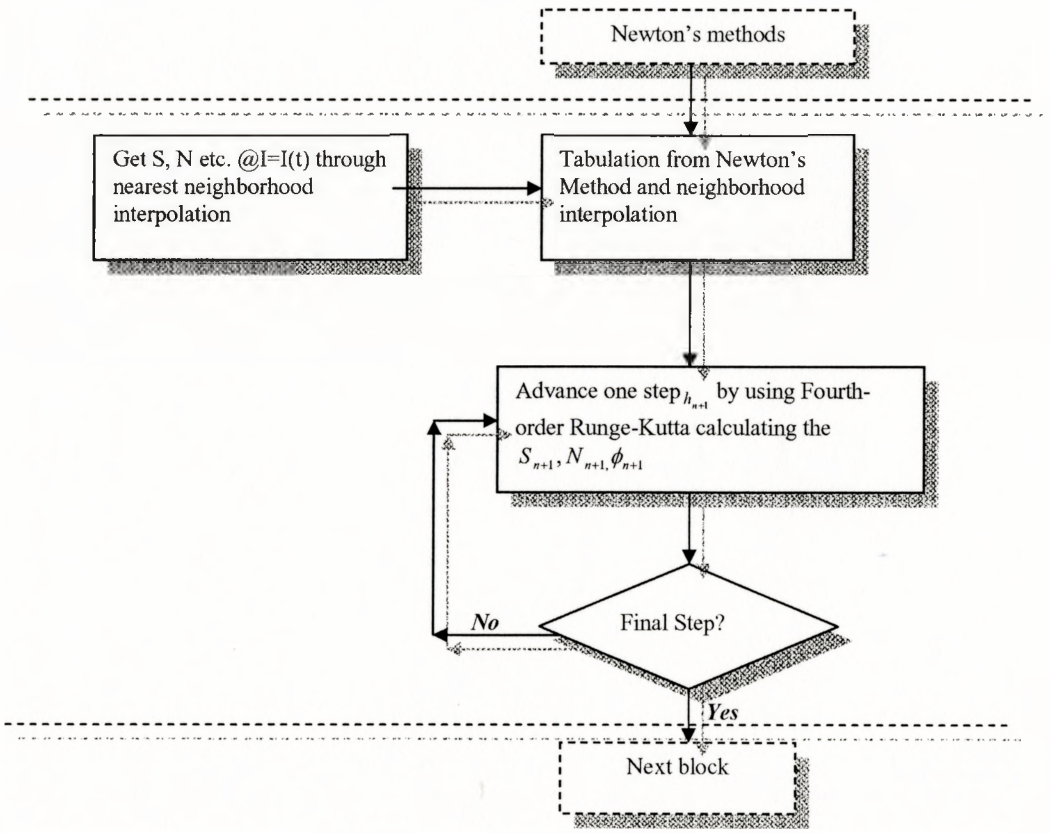

Figure 4-2 Data flow of dynamic solution

The fifth-order Runge-Kutta with adaptive control implementation steps, which is similar to implementations in fourth-order Runge-kutta, but more precise, more accurate:

1. Look up the values of S_0, N_0 in the tabulation generated from steady state solution, corresponding to the output current from the previous block. If found in the tabulation, go to (3)

2. If not found, to find the closest two neighbours, do linear interpolation, calculating the values of S_0, N_0.

3. Calculate scaling S_{scale}, N_{scale} used to monitor accuracy, getting desired accuracy Δ_0

4. Advance one step h_{try}, Calculate fifth-order Runge-Kutta and fourth-order Runge-Kutta with six evaluations $S_{n+1}, N_{n+1,} \phi_{n+1}$.

5. Calculate error estimate Δ_1 as difference between fourth and fifth order method.

6. If $\Delta_0 > \Delta_1$, output the current results calculated by fifth-order Runge-Kutta, and calculated h_{next} for next step use.

   If $\Delta_0 < \Delta_1$, shrink current stepsize, and recalculate from step (4)

7. Check if the final step reached, if not, go to (3). If yes, exit the Runge-Kutta loop.

Below is the diagram of implementation of fifth-order Runge-Kutta with adaptive control.

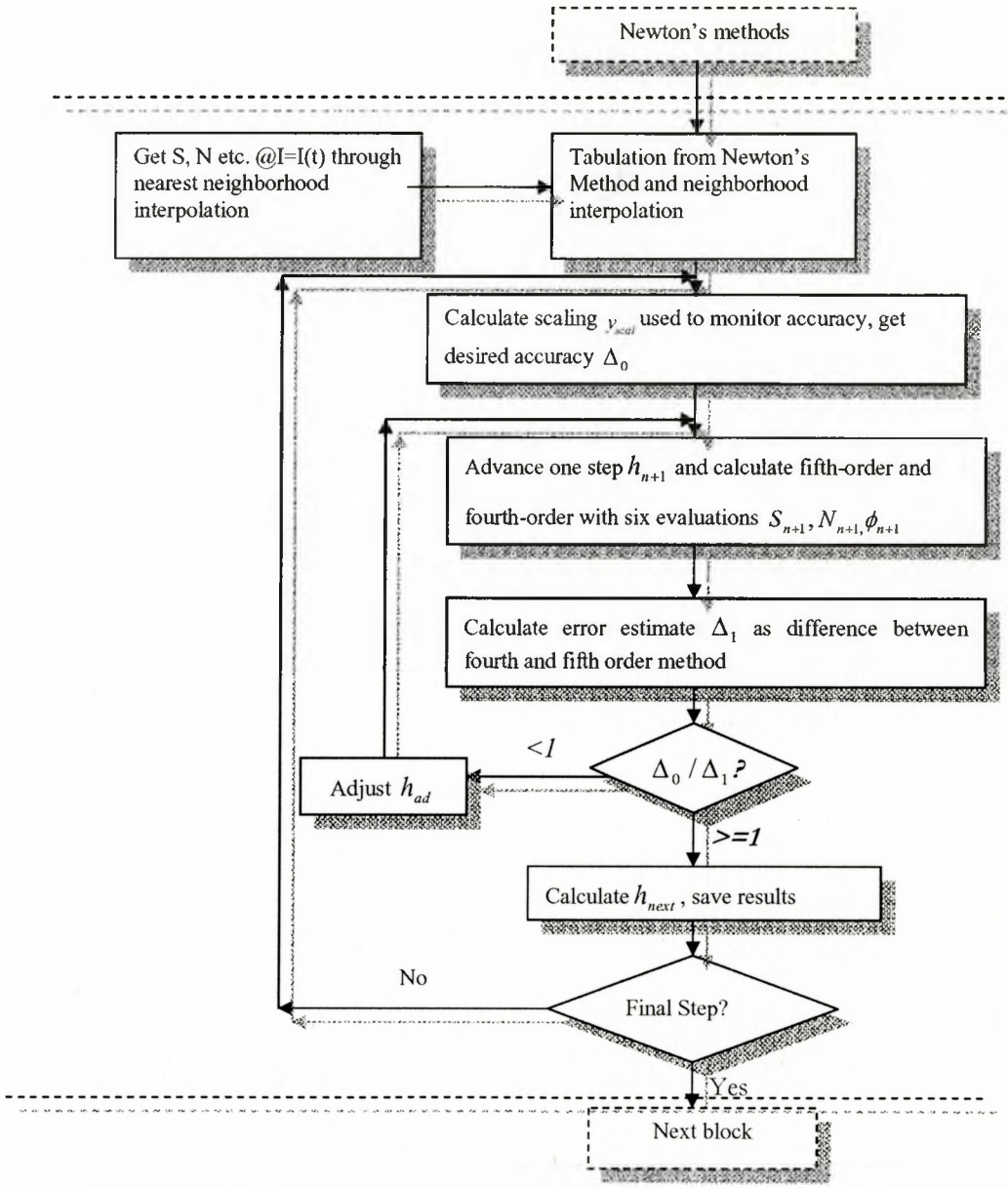

Figure4-3 Laser dynamic simulation implementation steps for Runge-kutta

Here combine all the numerical methods together to form a basic block of laser simulation, which can be used into more complex fashions when we simulate the whole optical transmission system.

1. load laser parameters;
2. Initialize all variables needed in the simulation according to parameters loaded;
3. Passing through Newton's Method;
4. Passing through Runge-Kutta Method.

Diagram showed below:

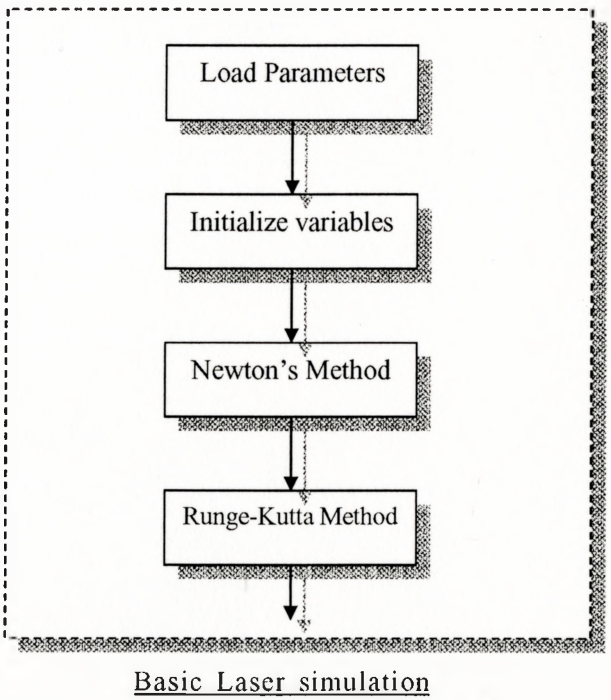

Figure 4-4 Data flow of solution of laser block

The more detailed laser simulation utilization of optical system will be discussed in later chapters.

CHAPTER 5

5 SIMULATION RESULTS

The steady state and dynamic simulations results for typical semiconductor lasers are presented in this chapter. The parameter selection method is also explained.

5.1 Parameter Selection

For multimode laser simulation, the gain for each optical mode is different. In previous chapter, we consider the gain profile has symmetrically parabolic shape. Therefore, we can get symmetrical lasing spectrum at output. Not every mode in laser cavity can get lasing unless it satisfies lasing conditions both in resonance condition and phase condition. Thus, from those conditions, we can calculate the possible number of lasing modes. It can determine apparently that our simulation is single mode simulation or multimode simulation based on changing the laser intrinsic parameters such as length of laser cavity. To describe more clearly, we put the equation here :

$$\delta\nu = c/(2L\bar{\mu}_{eff}) \text{ or } \delta\lambda = \lambda^2/(2L\bar{\mu}_{eff}) \quad \textit{Equation 5-1}$$

From above equation, we can find that, given the length L of the laser cavity, the mode spacing $\delta\nu$ is determined for certain material if we assume the effective group reflective index $\bar{\mu}_{eff}$ as a constant in simulation because of minor impact from the dispersion of material refractive index affected by optical frequency. Further, the number of possible lasing modes is determined as well because the gain profile is fixed when above lasing threshold with the consideration of linear gain with carrier density in laser cavity.

Other parameters will be further selected in the simulation in addition to the possible lasing modes. Below shows the table the parameters we are using in the simulation, which are obtained from real typical semiconductor laser parameters.

PARAMETER	SYMBOL	VALUE	UNIT
Cavity length	L	300	um
Active-region width	w	2	um
Active-region thickness	d	0.2	um
Confinement factor	Γ	0.3	
Effective group refractive index	$\overline{\mu}_{eff}$	3.9	
Line width enhancement factor	α_{LEF}	3	
Petermann's factor	K	1	
Cavity loss	α_{closs}	20	cm^{-1}
Population inversion factor	n_{sp}	2	
Gain coefficient for Bulk	a_{bulk}	3.0×10^{-16}	cm^2
Gain coefficient of Quantum well	a_{QW}	1000	cm^{-1}
Gain saturation factor	ε	2.0×10^{-17}	cm^3
Carrier lifetime	τ_n	1	ns
Photon lifetime	τ_p	3	ps
Carrier density at transparency	n_0	1×10^{18}	cm^{-3}
Gain width	$w_{gain-width}$	49.2	nm
Reference wavelength	λ_{ref}	1550.12	nm
Planck's constant	h	6.625×10^{-34}	$J\cdot s$
Electron charge	q	1.6×10^{-19}	C

Table 5-1 Typical parameter values for laser diode

From the parameters provided above, we can determine for our simulation, the laser supports 47 optical modes. Also we can get single mode operation when cavity length is decreased not to be larger than around $12.5\,um$.

5.2 Steady State Performance under Symmetrical Gain Assumption

We consider both linear gain and nonlinear gain simulations here, as we know, the term $1/(1+\varepsilon S_j)$ dominates the nonlinear feature in the simulation. Under single mode operation, the subscript j is set to be 1; under multiple modes operation, it is set to be the number of total number of possible lasing modes. In fact, the gain spectrum in reality shows some asymmetry. Under linear operation, the gain saturation factor ε is set to be 0; under nonlinear operation, it will be set to be the corresponding number appeared in *Table 5-1.*

5.2.1 Multimode Behavior under Linear Gain Assumption

In reality, for practical Fabry-Perot Lasers with bulk material or Quantum well structure, it is difficult to get a purely single lasing mode. Instead, we can observe multiple laser modes spontaneously. The reason that we introduce the single mode consideration above is that we want to use the extreme case to explain the nonlinear gain approximation. Of course, we can obtain a single mode operation and corresponding simulations if the DFB (distribution feedback) laser is employed. However, DFB laser is another topic which is discussed in other's writings. In our simulation, we only consider traditional Fabry-Perot laser with Bulk or Quantum well structures.

In the following, we will continue discussing and show some results of the linear and nonlinear gain approximations under multiple modes operations.

In *Figure 5-1*, *Figure 5-2*, we just plot first 17 lasing modes, actually there are more than 17 lasing modes lasing out from the laser structure as we defined in *Table 5-1*. Under linear gain approximation, only the first mode ($m = 0$) increases with the injection current, other side modes reach into saturation state after threshold. And also the first mode is almost linear with the injection current after threshold, and carrier density in laser cavity keeps in constant. It demonstrates that the gain under linear consideration is constant after threshold and thus the optical power is linear proportion to the injection current. *Figure 5-2* shows the optical output change with injection current in logarithm scale in which the modes saturation and the first mode more are observed. *Figure 5-3* shows the carrier density change with injection current. It clearly indicates that after threshold, the carrier reach saturation promptly. *Figure 5-4* shows the wavelength shift with the change of carrier density in along different injection currents. The wavelength change is relative to the reference wavelength at transparency point.

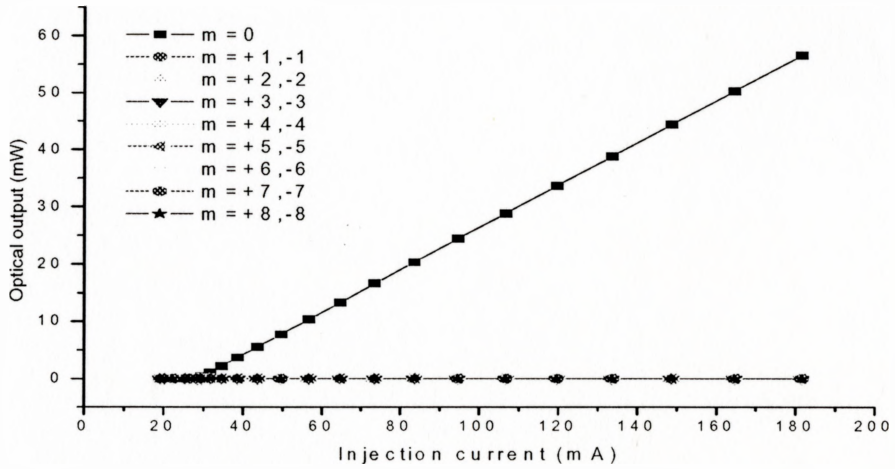

Figure 5-1 Optical output V.S. injection current in multi-mode operation under steady state presented by linear scale

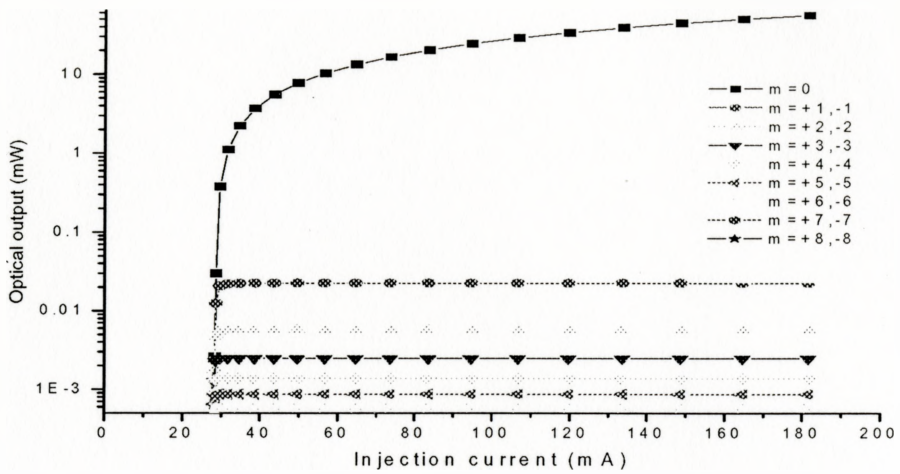

Figure 5-2 Optical output V.S. injection current in multi-mode operation under steady state presented by logarithm scale

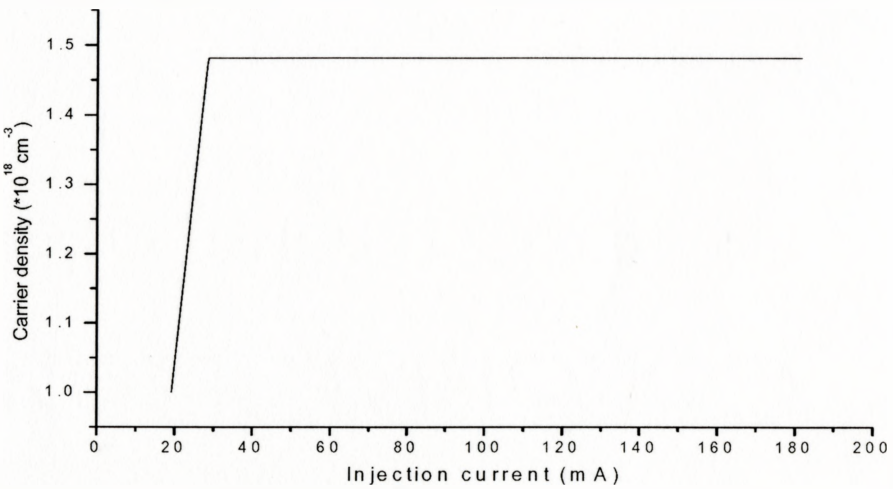

Figure 5-3 Carrier density V.S. injection current for multi-mode steady state

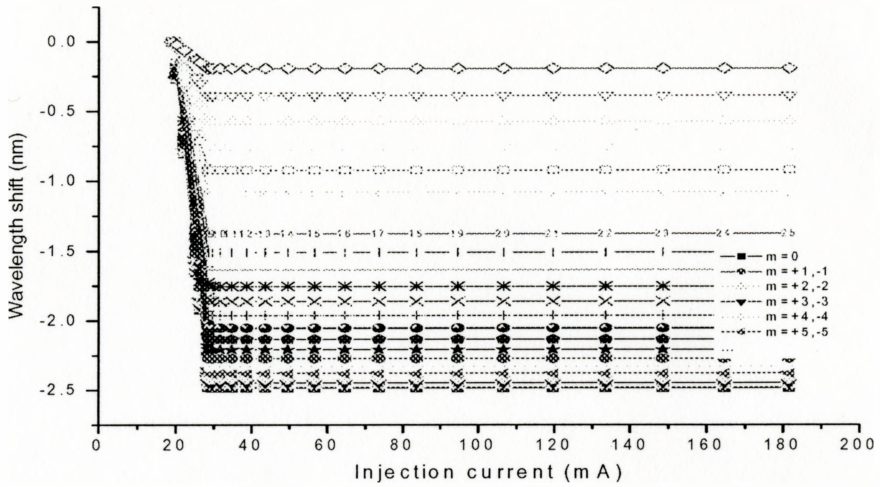

Figure 5-4 Wavelength shift V.S. injection current

5.2.2 Multimode Behavior under Nonlinear Gain Assumptions

Under nonlinear gain simulation, because of gain saturation occurring in the laser cavity, we can see several side modes get lasing. As the injection current increases, the more and more side modes get lasing because of the spectral hole burning, which can be explained that the gains for the first lasing mode is saturated, even depressed under heavy photon number existing in cavity, therefore the side modes get lasing because of the gain depression of central wavelength, or first mode. From *Figure 5-5*, under moderate current injection, there are around seven modes lasing. And with the increase of injection current, the other high-order side modes also get lasing. From *Figure 5-6*, because of the nonlinear gain, the carrier density in laser cavity does not keep constant any more after the lasing threshold, but it slightly increases with the injection current. The hole burning phenomenon has been exhibited out from the figures of photon output and carrier density. In *Figure 5-9*, the wavelength shift with the injection current does slightly decease after the threshold.

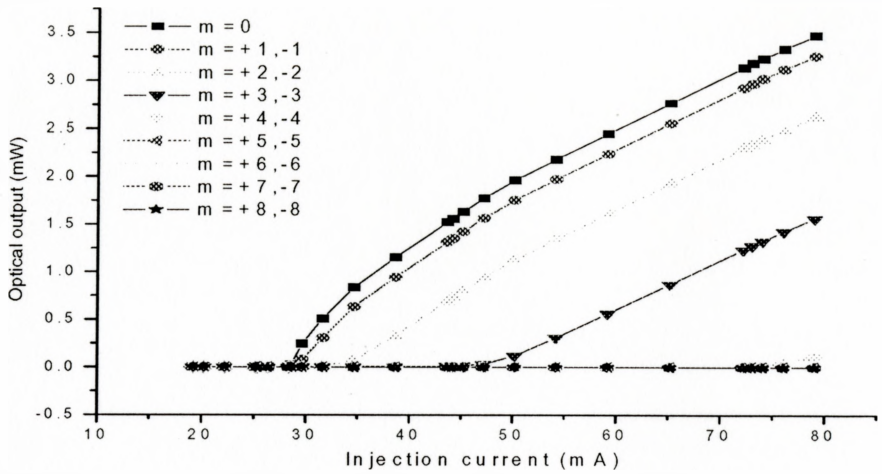

Figure 5-5 Optical output V.S. Injection current in multi-mode operation under steady state presented by linear scale

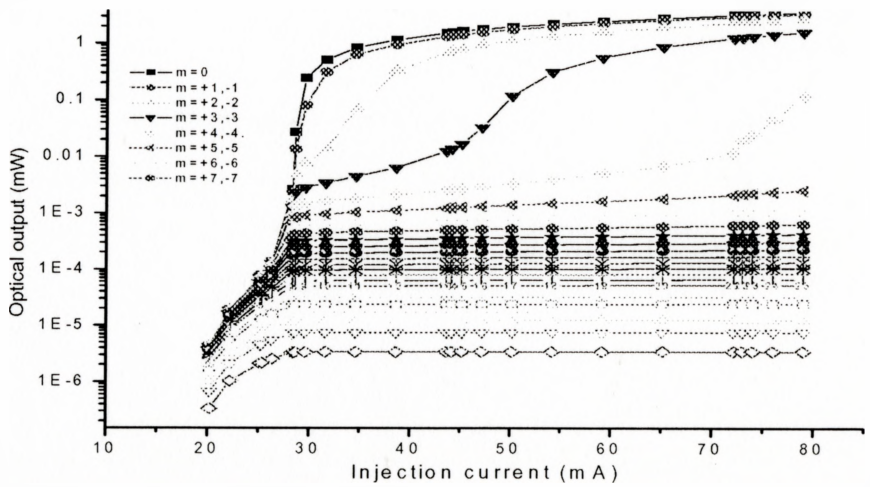

Figure 5-6 Optical output V.S. injection current in multi-mode operation under steady state presented by logarithm scale (Bulk)

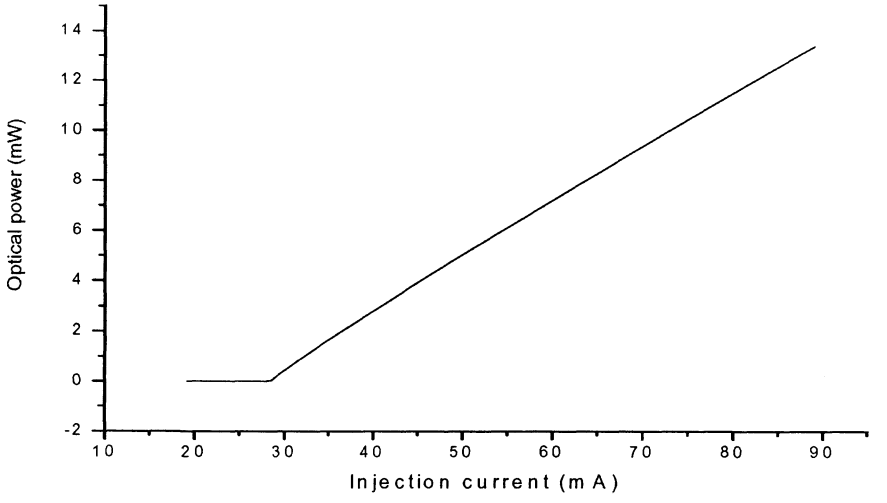

Figure 5-7 Optical power with summation of all modes V.S. injection current for steady state (Bulk)

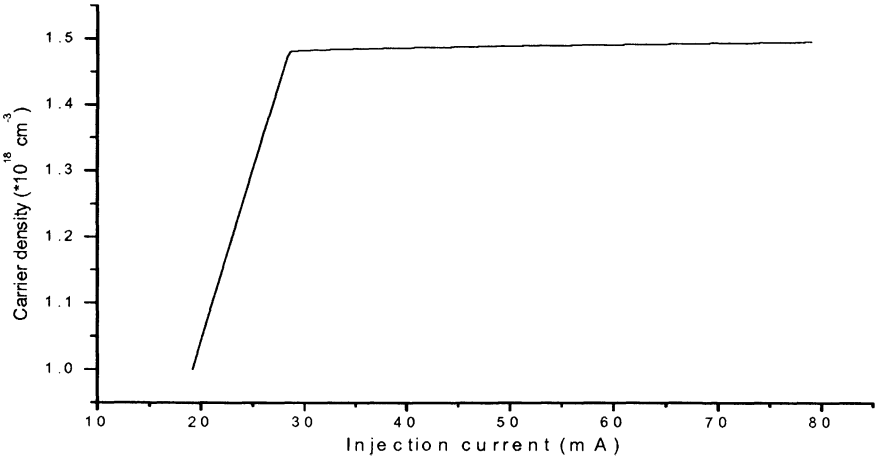

Figure 5-8 Carrier density V.S. injection current for multi-mode steady state

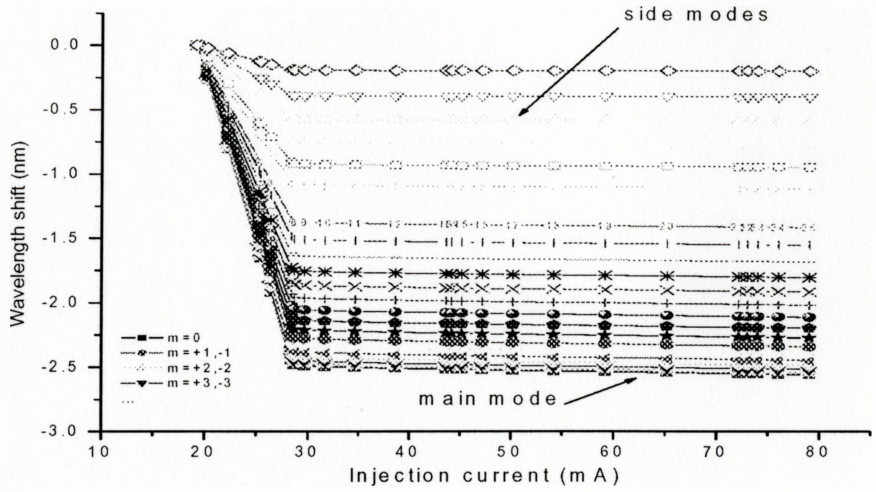

Figure 5-9 Wavelength shift V.S. injection current

Till now, we only discuss the bulk material based Laser diode simulation. If we changed the structure of the laser diode, what will it bring to us? Of course here, we didn't take the detailed quantum well features into our cases. Instead, we just consider the QW from the gain constant point of view. For detailed quantum well laser semiconductor, please refer to the corresponding papers or books [5] [22].

With the comparison of the bulk and quantum well simulations, in addition to the almost similar simulation results. it is found that quantum well based laser diode can get lasing with relatively low injection current and relatively small carrier density in cavity, which means quantum well based laser diode has superior performance than to traditional bulk material based laser diode. In *Figure 5-10*, *Figure 5-11*, *Figure 5-12*, the steady solution of photon, carrier and wavelength shift has been shown.

All above is what we get from Steady state solution based on adaptive Newton Method. From the output of simulation, we get very reasonable results which match the corresponding text book, or paper well. Next, we will continue to discuss the simulation results coming from transient response.

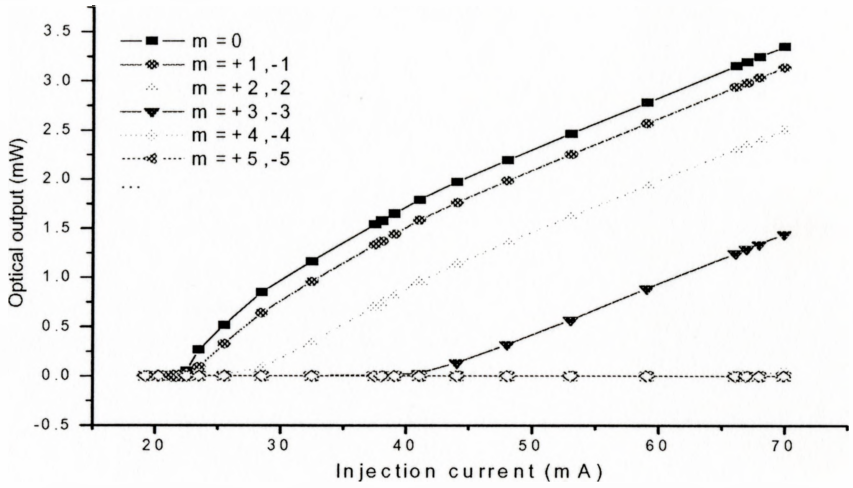

Figure 5-10 Optical output V.S. injection current in multi-mode operation under steady state in quantum-well structure laser (here only first 11 modes presented)

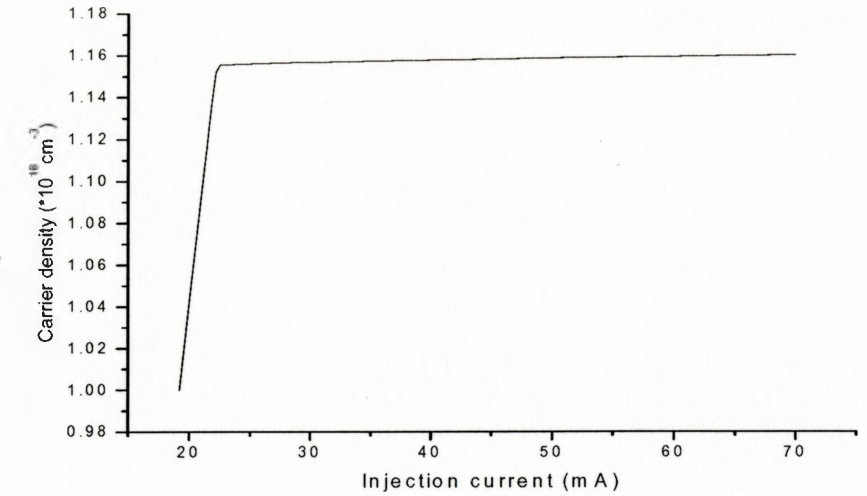

Figure 5-11 Carrier density V.S. injection current for quantum well

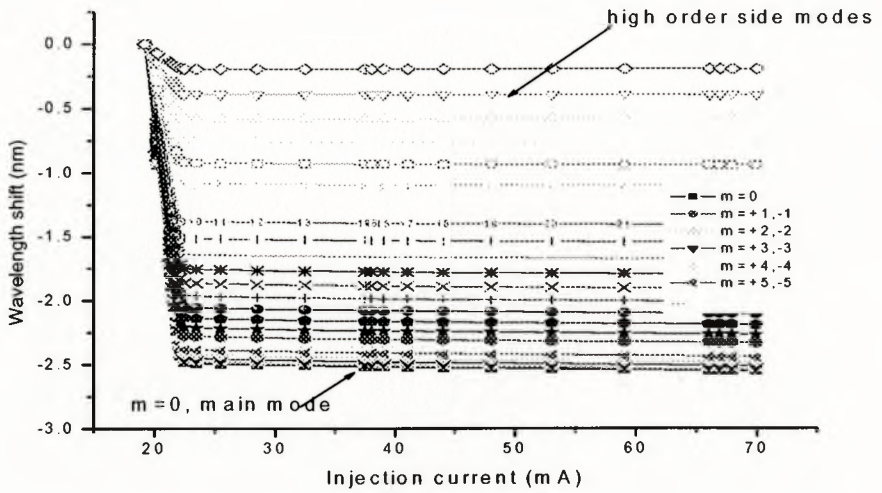

Figure 5-12 Wavelength shirt for quantum well

5.3 Dynamic Performance

Based on the multiple mode rate equations, we can employ Runge-Kutta method to simulate the transient response of laser diode. In previous chapter, we did discuss the detailed the implementation steps. So here we will directly validate the simulation results.

Figure 5-13 shows us a 4-bit stream which has the pattern of "0110", which is in the format of NRZ.

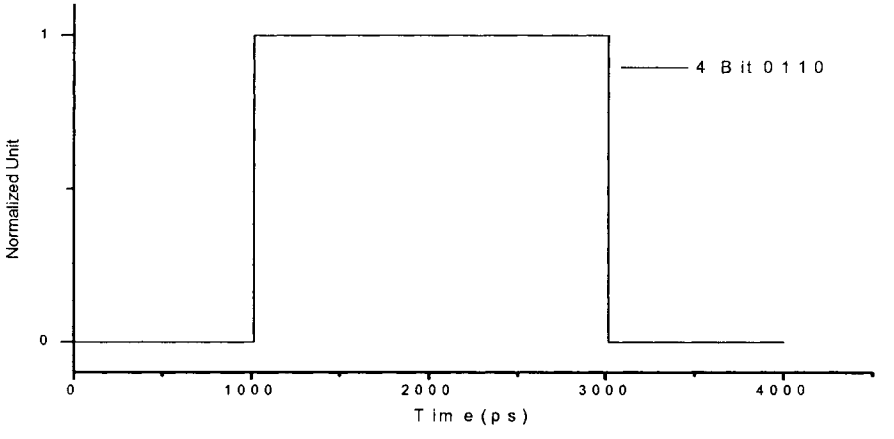

Figure 5-13 Sampling at 15.625ps for 1Gb/s transmission rate

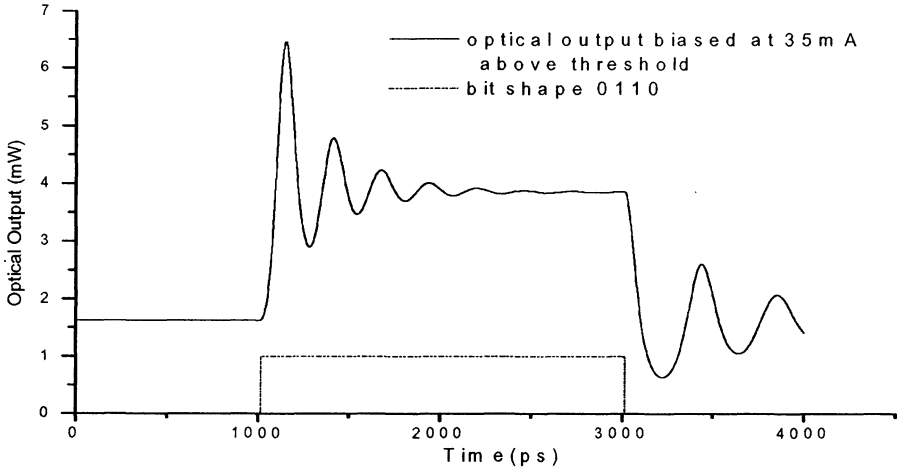

Figure 5-14 Optical output under the condition: biased at 35mA and modulation current is 10mA, sampling at 15.625ps for 1Gb/s transmission rate

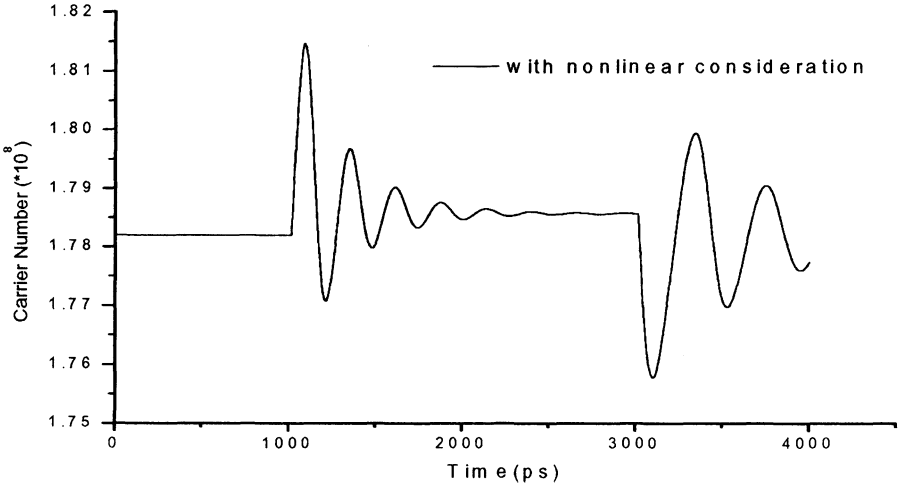

Figure 5-15 Carrier density under the condition: sampling at 15.625ps for 1Gb/s transmission rate

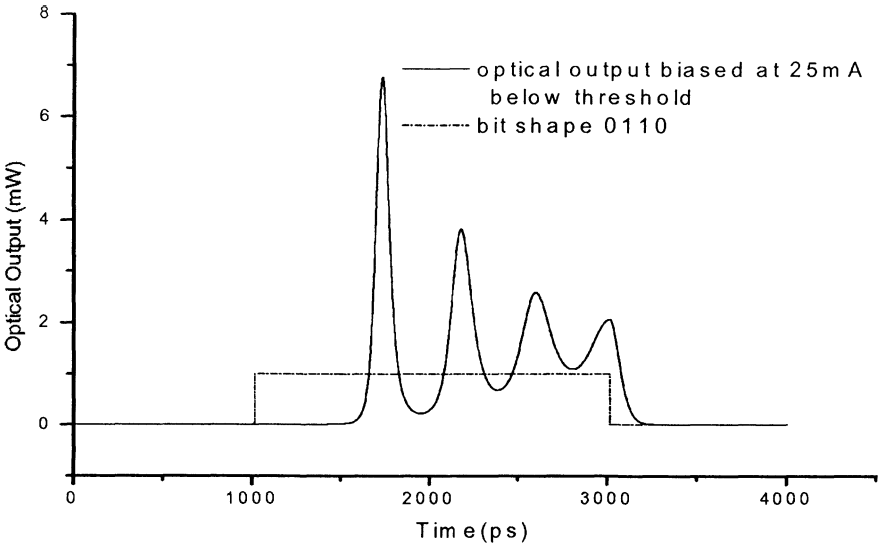

Figure 5-16 Optical output biased below the threshold

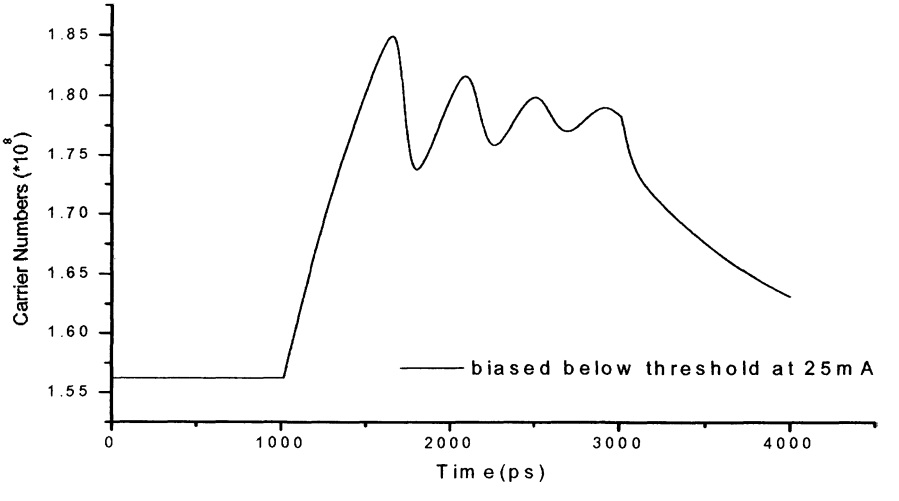

Figure 5-17 Carrier density change biased below the threshold

In the scenario of above-threshold bias modulation in *Figure 5-14* and *Figure 5-15*, we simulated the 0110 4-bit stream in 1 GB/s transmission rate. The sampling period is 15.625 pico-seconds. The bias current is 35mA above the threshold and modulation current is 10mA. In the *Figure 5-14* the optical power emitted gets oscillation around its steady state, thus reaching steady state. From *Figure 5-15* also we can see the carrier density in cavity oscillated and reached steady state afterwards.

Figure 5-16 shows the 0110 stream response biased at 25mA below the threshold. There is a longer turn-on delay before lasing than the case of above-threshold bias modulation. And also the carrier number in both examples has big difference. We explain as: if the bias is below the threshold, the carrier population in laser cavity is lower than carrier populations at threshold. Only if carrier population increases to the threshold carrier populations, the laser can get lasing, which means population inversion is reached. To reach the population inversion, it takes longer time for under-threshold case to accumulate the carrier population in cavity. Comparing with the bias above the threshold situation, there is no carrier collection time in it. So we will observe the longer time turn-on delay. In high speed optical transmission system, this kind of turn-on delay is not acceptable, so normally we also bias the laser above the threshold in operation.

Besides the turn-on delay, we can observe the photon and carrier oscillation phenomena in both situations before their steady state reached, which are caused by the intrinsic nonlinear characteristic of the semiconductor laser, namely, relaxation oscillation. The relaxation oscillation affects the modulation performance of laser diode in optical communication. From our dynamic response simulation, we can get the relaxation frequency of our specified laser diode by converting the pulse stream from time-domain into frequency domain using Fourier transform.

After getting the optical output in time domain, we can use Fast Fourier Transform (FFT) to get the frequency spectrum of optical output. In *Figure 5-18*, the modulation current is 1mA, and bias currents are 60mA, 80mA, 100mA, and 150mA. After FFT, the oscillation frequency for each injection current is observed. And for a certain laser, the relaxation oscillation frequency moves towards to higher frequency when the bias current increases. The sampling interval here is 15.625 pico-seconds.

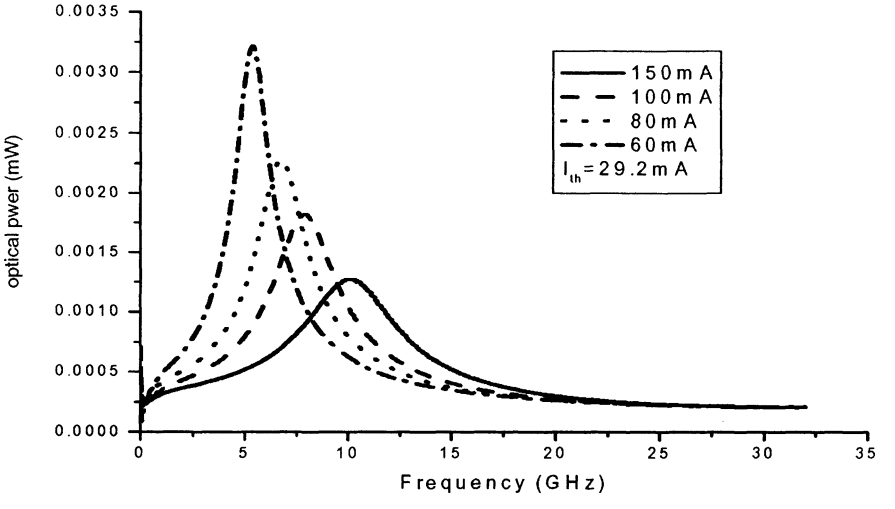

Figure 5-18 Amplitude response under injection current 60mA, 80mA, 100mA, 150mA (Bulk)

The following three figures *Figure 5-19,Figure 5-20,Figure 5-21*, show a 16-bit stream internally modulated under 10Gb/s, 1Gb/s, 0.1Gb/s respectively. Those figures demonstrate that the optical pulses get worse with increase of modulation speed. For internal modulation, which directly modulates bias current, the relaxation oscillation will eternally determine the maximum modulation bandwidth. Therefore, if we want a high modulation bandwidth in high speed optical transmission system, the external modulation scheme is usually employed.

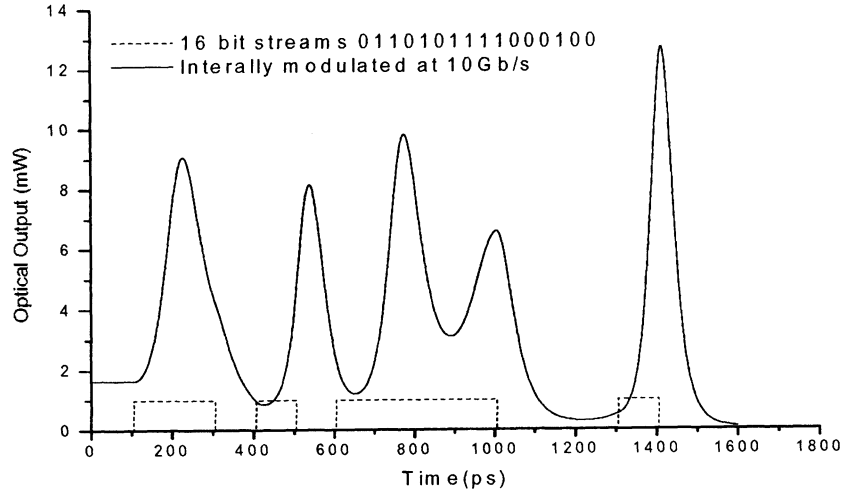

Figure 5-19 Optical pulse modulated at 10Gb/s

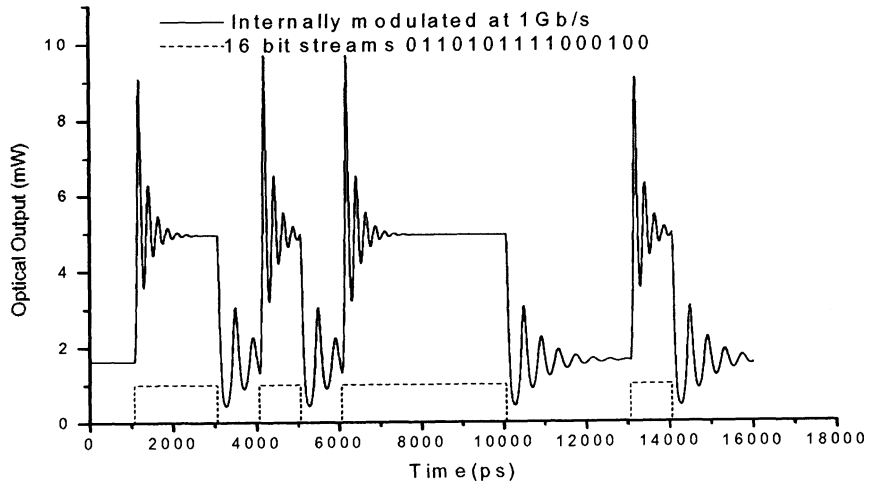

Figure 5-20 Optical pulse modulated at 1Gb/s

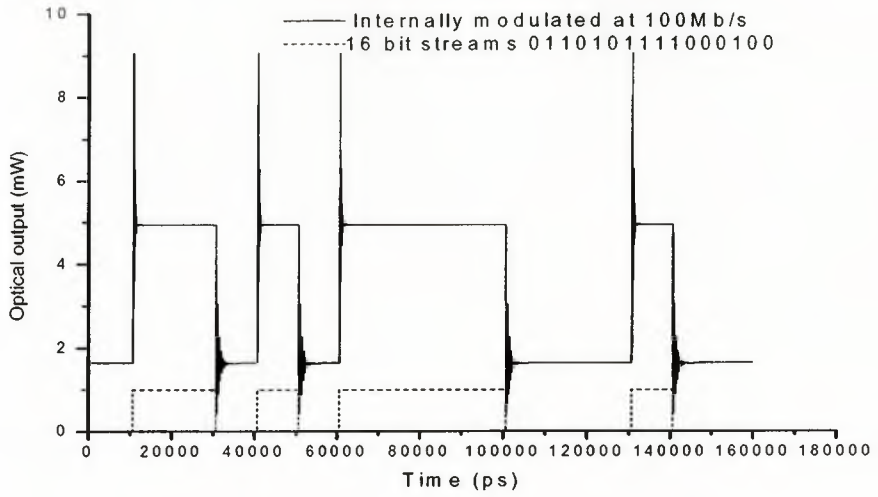

Figure 5-21 Optical pulse modulated at 100Mb/s

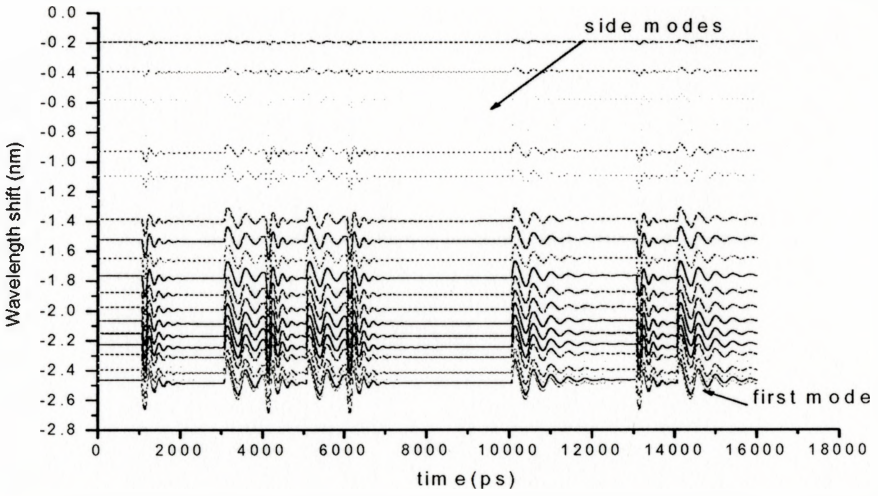

Figure 5-22 Wavelength shift at 1Gb/s with bias of 35maA and modulation current of 15mA

In *Figure 5-22,* the wavelength shift is plotted with the power change of optical pulse which is internally modulated at 1Gb/s.

The above discussion does not take semiconductor noises into account. So in next chapter, we will further add noise terms into our rate equations to get more real laser simulation model for semiconductor laser.

CHAPTER 6

6 NOISE CHARACTERISTICS

So far, we have simulated the laser performance in time domain, i.e., the waveform of the output optical power and lasing frequency, without noise consideration. However, semiconductor laser is a device driven by the spontaneous emission noise. The spontaneous noise will bring in fluctuations on both of the optical intensity (photon numbers) and lasing frequency, known as the relative intensity noise and the phase noise, respectively. These noises may bring in significant effect in some applications or al least introduces additional penalty in the optical links. To have the noise characteristics included in our model, we have to firstly modify the governing equations and secondly resolve them.

6.1 Noises Incorporated Model

The noise modeling through single mode rate equation has already been discussed in [8]. The noise characteristics can readily be obtained by following an approach similar to the small signal analysis [9] [10].

Following the same methodology, we directly add the noises arising from the spontaneous emission to the photon number and phase rate equations and the shot noise from the carrier recombination to the carrier rate equation by taking the noise contribution all in the form of Langevin driving force [11] [12]. Our governing equations, therefore, become:

$$\frac{dS_j(t)}{dt} = S_j(t)[\Gamma v_g g_{m,j}(t) - \frac{1}{\tau_{p,j}}] + \Gamma K v_g n_{sp} g_{m,j}(t) + F_{s,j}(t), \quad j = 1,2,\ldots, \quad M$$

$$\frac{d\phi_j(t)}{dt} = \frac{1}{2}\alpha_{LEF}\,\Gamma v_g g_{m,j}(t) + F_{\phi,j}(t), \quad j = 1,2,\ldots, \quad M$$

$$\frac{dN(t)}{dt} = \frac{I(t)}{qV} - \frac{N(t)}{\tau_n} - \frac{\Gamma v_g}{V}\sum_{j=1}^{M} g_{m,j}(t) S_j(t) + F_N(t)$$

$$g_{m,j}(t) = a[N(t) - N_{tr}][1 - (j\frac{\delta v}{\Delta v})^2]/[1 + \varepsilon_j S_j(t)], \quad Bulk$$

$$g_{m,j}(t) = a \ln\frac{N(t)}{N_{tr}}[1 - (j\frac{\delta v}{\Delta v})^2]/[1 + \varepsilon_j S_j(t)], \quad QW$$

Equation 6-1

As result of the random Langevin driving force, S_j, ϕ_j, N all become random processes and the rate equations are stochastic equations. When the photon numbers and the carrier density are all at high level, as the random sources, all the noises can be approximated as the Gaussian process with zero mean according to the large number and the center-limit laws.

Under this assumption, the noises must satisfy the general relations set for the mean value and the correlation function:

$$\langle F_a(t)\rangle = 0$$

$$\langle F_a(t)F_b(t')\rangle = 2D_{ab}\delta(t-t')$$

Equation 6-2

where $a,b = S_j, \phi_j, N$, the angle brackets denote either sample average or time average as all the noises are stationary and ergodic. The coefficients D_{ab} are given as:

$$D_{(S,j)(S,j)} = \Gamma K v_g n_{sp} g_{m,j}(t)\langle S_j \rangle, \qquad D_{(S,j)(S,j')} = 0,$$

$$D_{(S,j)N} = -\Gamma K v_g n_{sp} g_{m,j}(t)\langle S_j \rangle, \qquad D_{NN} = \Gamma K v_g n_{sp} \sum \langle S_j \rangle g_{m,j}(t) + \frac{\langle N \rangle}{\tau_n},$$

$$D_{(\phi,j)(\phi,j)} = \Gamma K v_g n_{sp} g_{m,j}(t) / \left(4\langle S_j \rangle\right), \quad D_{(\phi,j)(\phi,j')} = 0,$$

$$D_{(\phi,j)(S,j)} = D_{(\phi,j)(S,j')} = 0, \qquad D_{(\phi,j)N} = 0.$$

Equation 6-3

In these expressions $\langle S_j \rangle$, $\langle N \rangle$ represent the steady state values of the photon numbers and the carrier density, respectively, and are obtained from the steady state analysis as discussed previously.

For random process with Gaussian distribution, its variance function can be linked to its auto-correlation function and its mean value through:

$$\sigma^2 x(t) = R_{XX}(t,t) - \mu^2 x(t) \quad \textit{Equation 6-4}$$

where R_{XX} stands for the autocorrelation function of the random process $X(t)$ when $t_1 = t_2 = t$, σ_X the variance (mean square root) of the random process $X(t)$ at time t, and μ_X the mean value. Therefore, we have:

$$\sigma^2_{S,j} = 2\Gamma K v_g n_{sp} g_{m,j}(t)\langle S_j\rangle\delta(\tau)$$

$$\sigma^2_{\phi,j} = \Gamma K v_g n_{sp} g_{m,j}(t)\delta(\tau)/\left(2\langle S_j\rangle\right)$$

$$\sigma^2_N = 2\Gamma K v_g n_{sp}\sum\langle S_j\rangle g_{m,j}(t)\delta(\tau) + \frac{2\langle N\rangle}{\tau_n}\delta(\tau)$$

Equation 6-5

In our simulation, the random processes are modeled by the random number generators having the Gaussian distribution with zero means and variances given in *Equation 6-5*. Following steps have been implemented:

1. Initiate three independent random code generators, two are independent Gaussian distributed with zero mean and the standard deviation of one; the other is uniform distributed with derivation between 0 and 1.
2. Take Gaussian distributed random numbers to simulate the photon noise part and carrier noise part; take the uniform distributed random number as the random number to simulate the phase noise part.
3. Multiply the photon noise part with the standard deviation of photon noise as the random photon noise; multiply the carrier noise part with the standard deviation of carrier noise as the random carrier noise; multiply the standard deviation of phase noise part with the standard deviation of phase noise as the random phase noises.

6.2 Noise Simulation Result

Figure 6-1 shows the time domain simulated power fluctuations of the total lasing modes with the steady state power around 11.16mW. The variance of the fluctuation is comparable with the value observed in [25].

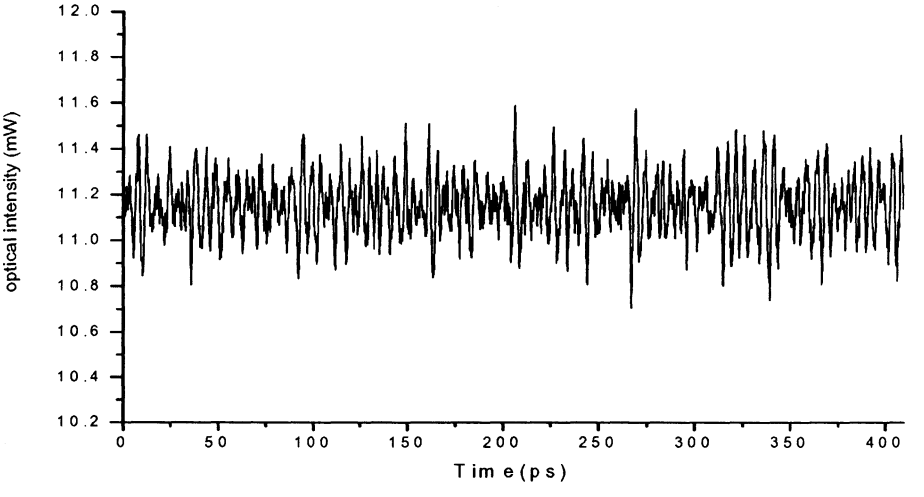

Figure 6-1 Simulated time domain optical power fluctuations with the average value of 11.16mW

6.2.1 Intensity Noise

After performing the Fourier transform through FFT, we obtain the noise characteristics in frequency domain. *Figure 6-2* shows the relative intensity noise spectra at several different injection currents. It shows that, unlike the white noise with a uniformly distributed spectrum, the relative intensity noise exhibits a peak near its relaxation

oscillation frequency. It is also observed that at certain frequency, the relative intensity noise decrease with the increased injection current.

6.2.2 Frequency Noise

Figure 6-3 gives the carrier noise spectrum when the bias current is set at 60mA. It clearly shows that, again, the carrier noise has a peak coincident with the relaxation oscillation frequency.

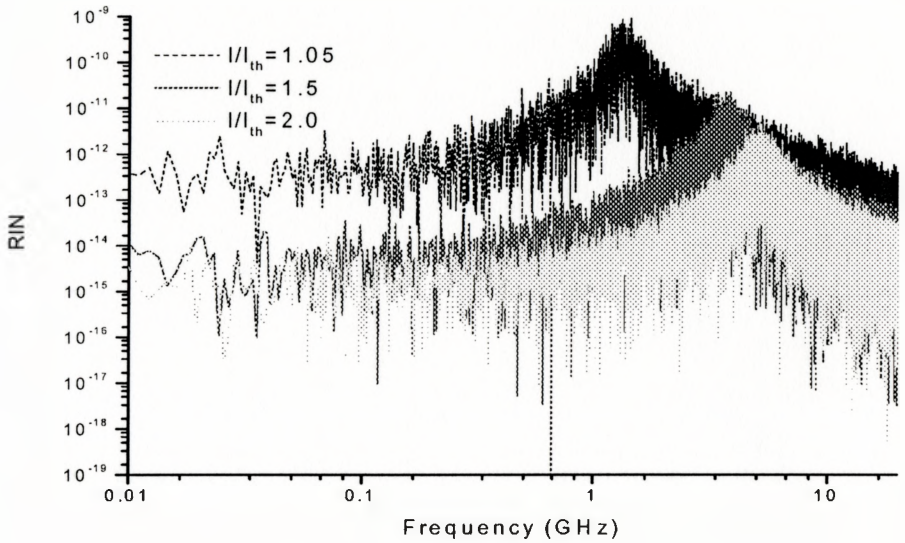

Figure 6-2 Simulated relative intensity noise spectrum at different bias current

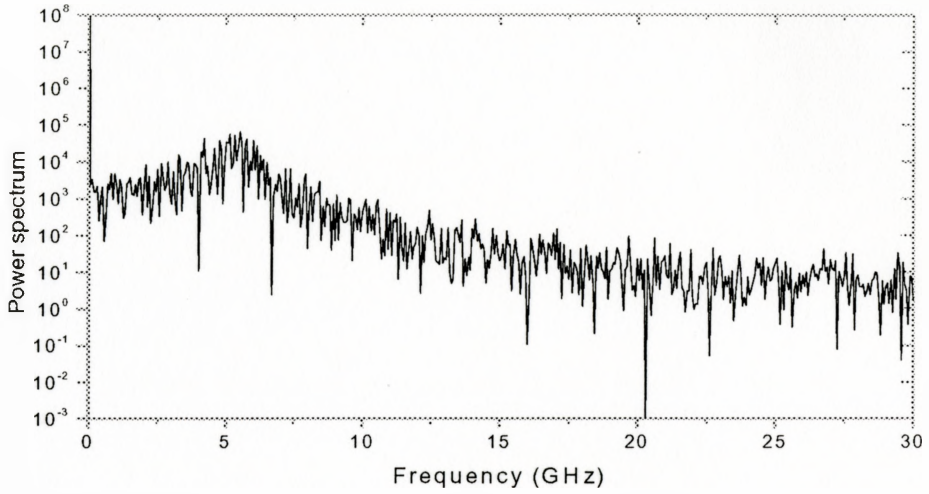

Figure 6-3 Simulated carrier noise spectrum

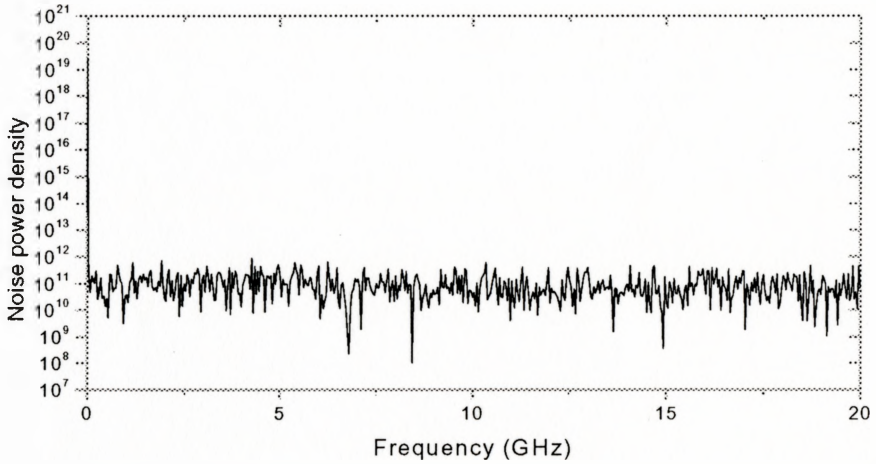

Figure 6-4 Simulated frequency noise spectrum for dominant driving phase noise

Figure 6-4 shows the calculated frequency noise spectrum of the 1st lasing mode at the same bias current (40mA). There is no peak appears due to the dominant white phase noise term (Langevin driving force in the phase rate equation) smears it out. By intentionally set this phase driving noise to zero, shown in *Figure 6-5*, we find the frequency noise peak at the relaxation oscillation frequency again as expected. From these results, we find that the frequency fluctuation will have a white noise spectrum if the phase noise driving component is dominant. On the other hand, the frequency noise spectrum will take a similar profile as the one we find for the RIN or carrier, with a peak positioned at the relaxation oscillation frequency, if the other carrier noise driving component is dominant. The former happens when the lasing mode power is small while the latter will happen when the linewidth enhancement factor is large enough.

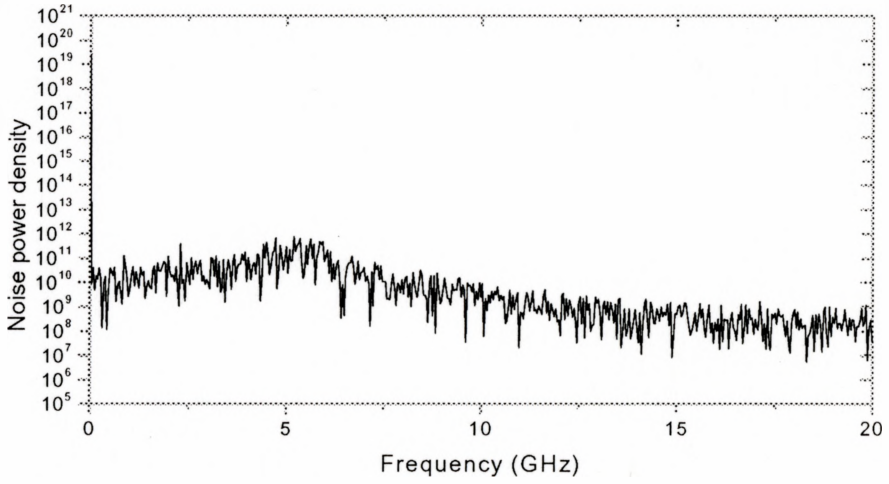

Figure 6-5 Simulated frequency noise spectrum for zero driving phase noise

CHAPTER 7

7 SIMULATION OF OPTICAL LINKS

Our ultimate goal is to develop a platform for the performance simulation of the point to point multi-channel optical links [17]. With all the device level simulators available, we present our simulation results for optical links with different configurations.

The numerical solvers for different component in the optical links are developed as individual modules. This allows us to establish the system platform with high flexibility. For different optical links, we have the system configuration and parameters specified globally and then have each individual component specified in the local module. Following this approach, we can readily handle any type of optical links.

Our system level simulation platform is made of the Random Code Generator (RCG) that provides the source of the bit stream in pseudo-random form, Laser Diode Simulator (LDS) that simulates the conversion of the signal in electrical domain into the signal in optical domain, Modulator Simulator (MOS) (optional, for external modulation scheme only) that simulates the signal modulation process, Optical Amplifier Simulator (OAS) that simulates the signal amplification process, Optical Fiber Simulator (OFS) that simulates the optical signal transmission and Photo-Detector Simulator (PDS) that simulates the conversion of the signal in optical domain back into the signal in electrical domain. All these simulations are performed in time-domain, following a scheme know as the real-time data-flow. The system simulation platform is illustrated by the block diagram shown in *Figure 7-1*.

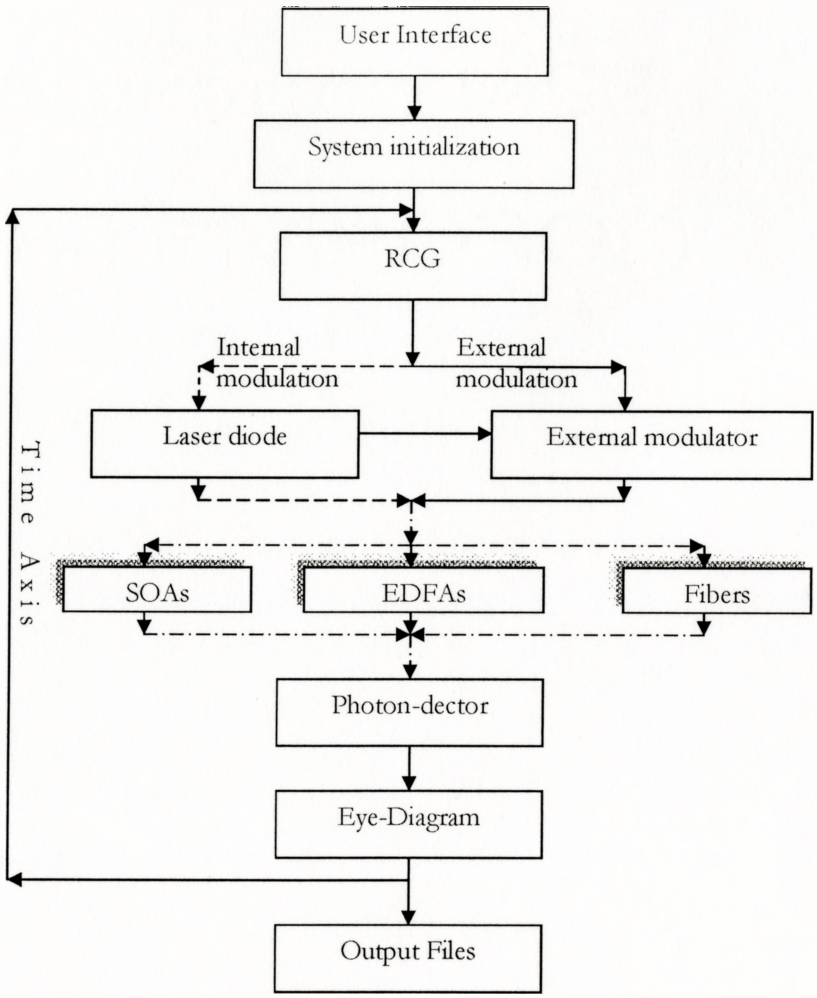

Figure 7-1 System simulation platform in real-time data-flow scheme

7.1 Case 1: Simple Back-to-Back Configuration

In order to evaluate the laser performance in optical links, we firstly simulate the system with back-to-back configuration shown as *Figure 7-2*. The laser parameters are selected the same as those given in *Table 5-1*. The simulated eye-diagrams are given in *Figure 7-3* and *Figure 7-4* for Gaussian-shaped and rectangular-shaped signal pulse generated by the RCG, respectively. In both cases, the laser is biased at 35mA and modulated by signals with a dynamic range of 50mA.

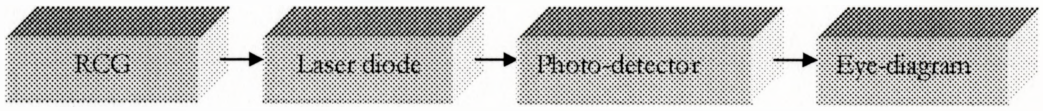

Figure 7-2 Back-to-back configuration diagram

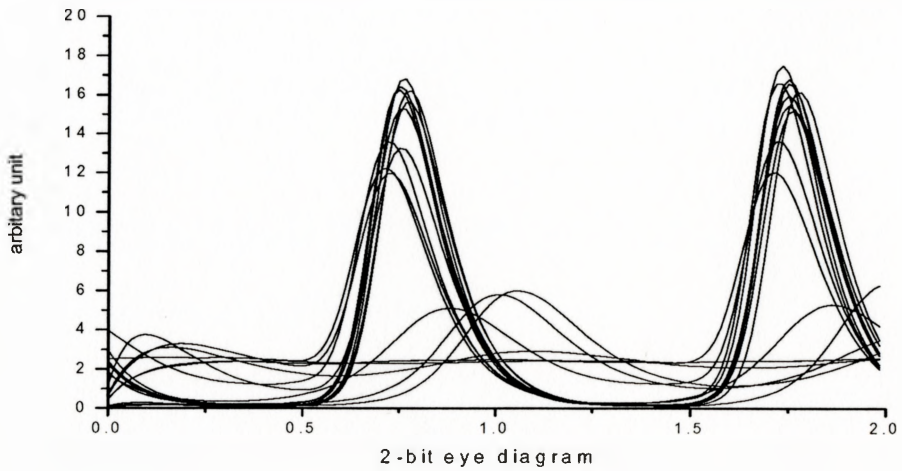

Figure 7-3 Back-to-back eye-diagram when laser is directly modulated by Gassian-shaped pulse stream at 2.5Gb/s

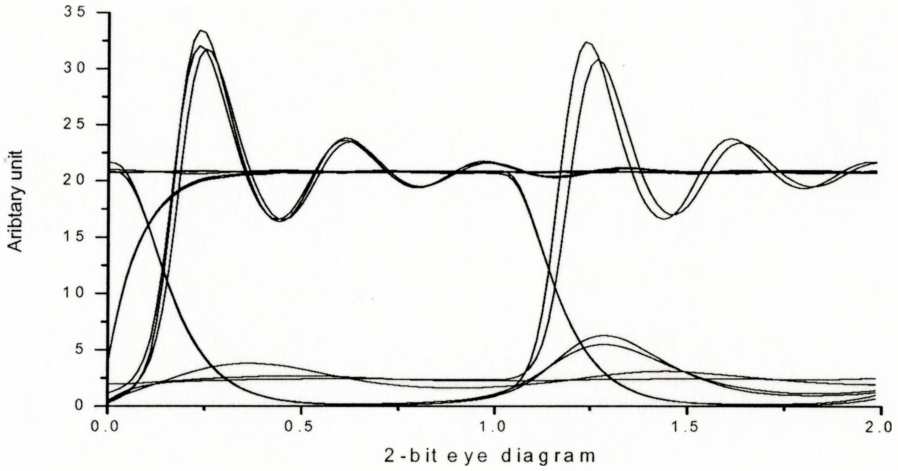

Figure 7-4 Back-to-back eye-diagram when laser is directly modulated by rectangular-shaped pulse stream at 2.5Gb/s

7.2 Case 2: CWDM 4 Channels with Direct Modulation at 1550nm Window

The system parameters in this simulation case are shown below. All optical devices' parameters are listed in Appendix.

System Parameters:

Number of Channel:	4
Bit-rate:	2.5Gb/s
Channel Spacing:	400GHz
Number of Frame(s):	4
Bit per Frame:	16
Optical Bandwidth:	C-band (1530nm-1563nm)
Source Shape:	Gaussian Pulse
Fiber Length:	60 km

System Configuration:

Figure 7-5 shows the block diagram for this simulation case.

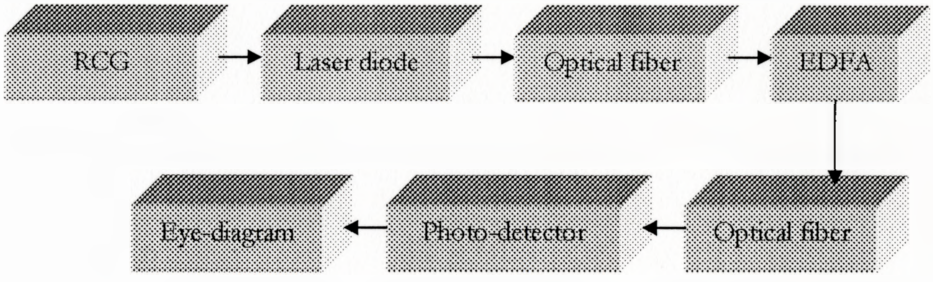

Figure 7-5 Block diagram for 2.5Gb/s CWDM scheme

The components in the test are Laser diodes, Fibers, EDFA and Photo-detector. All simulation parameters will be attached in appendix. The results about the laser part are in following fugures: *Figure 7-6, Figure 7-7, Figure 7-8.*

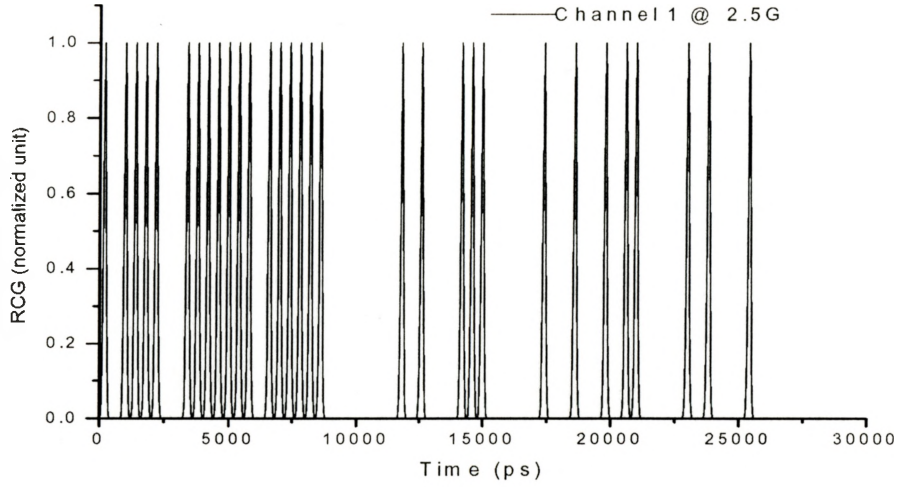
Channel 1 @ 2.5G
RCG (normalized unit)
1.0
0.8
0.6
0.4
0.2
0.0
0
5000
10000
15000
20000
25000
30000
Time (ps)

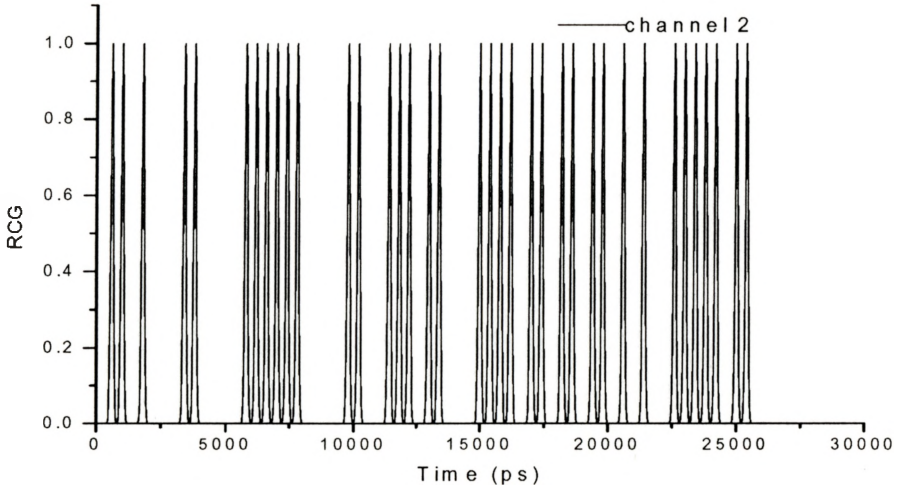
channel 2
RCG
1.0
0.8
0.6
0.4
0.2
0.0
0
5000
10000
15000
20000
25000
30000
Time (ps)

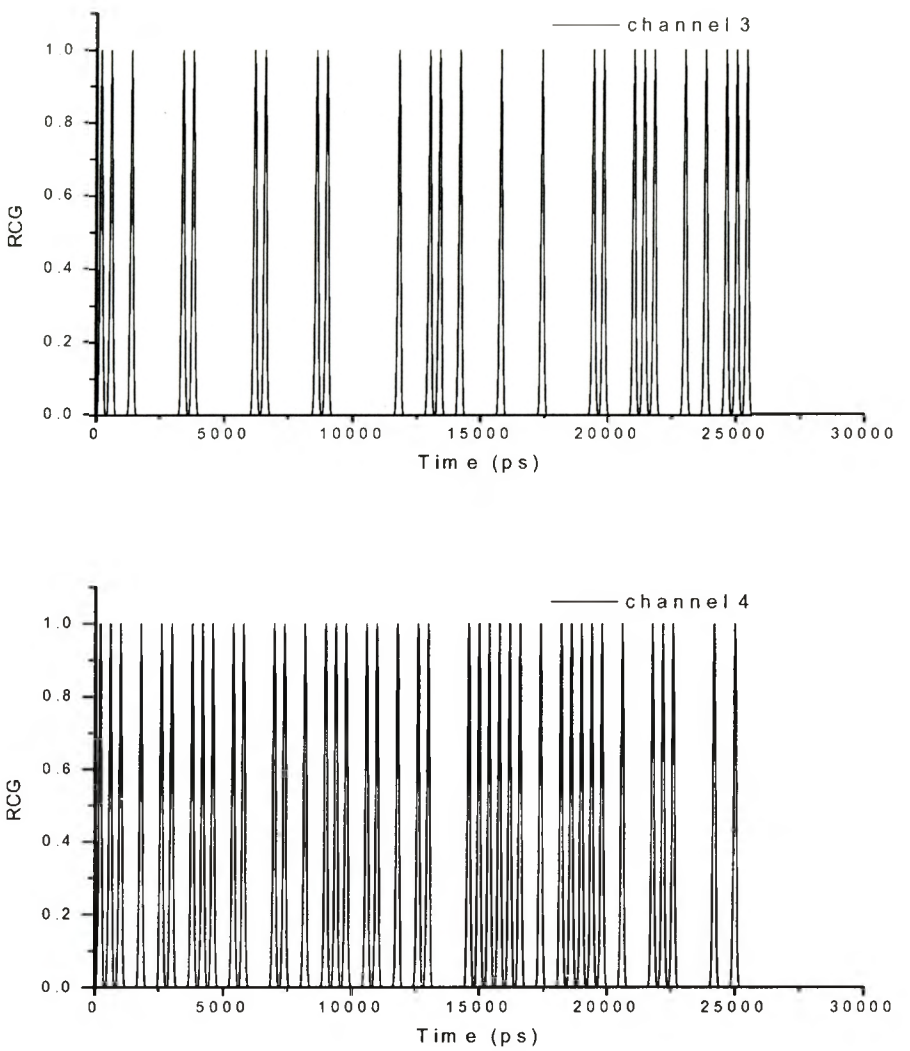

Figure 7-6 Output of RCG at 2.5Gb/s showing different patterns in different channels

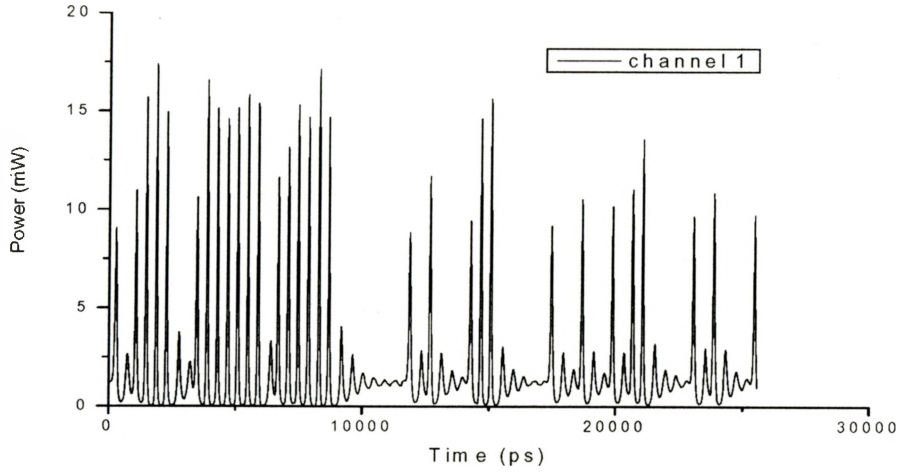
channel 1
Power (mW)
Time (ps)
0
5
10
15
20
0
10000
20000
30000

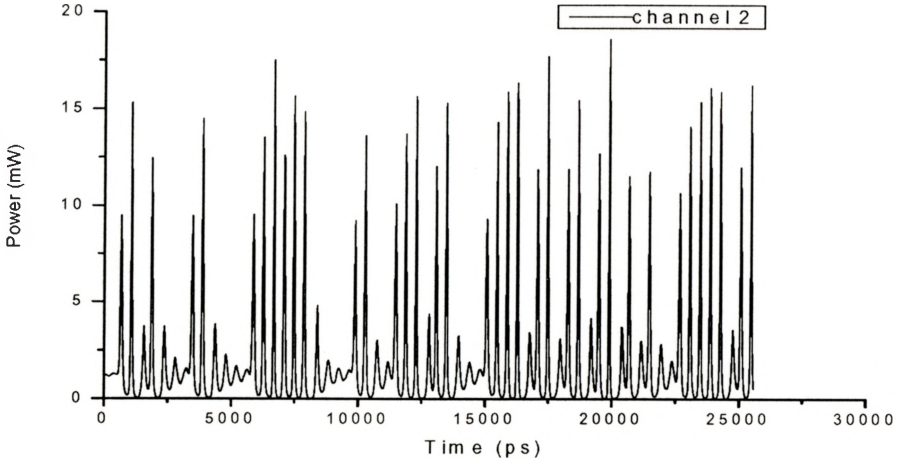
channel 2
Power (mW)
Time (ps)
0
5
10
15
20
0
5000
10000
15000
20000
25000
30000

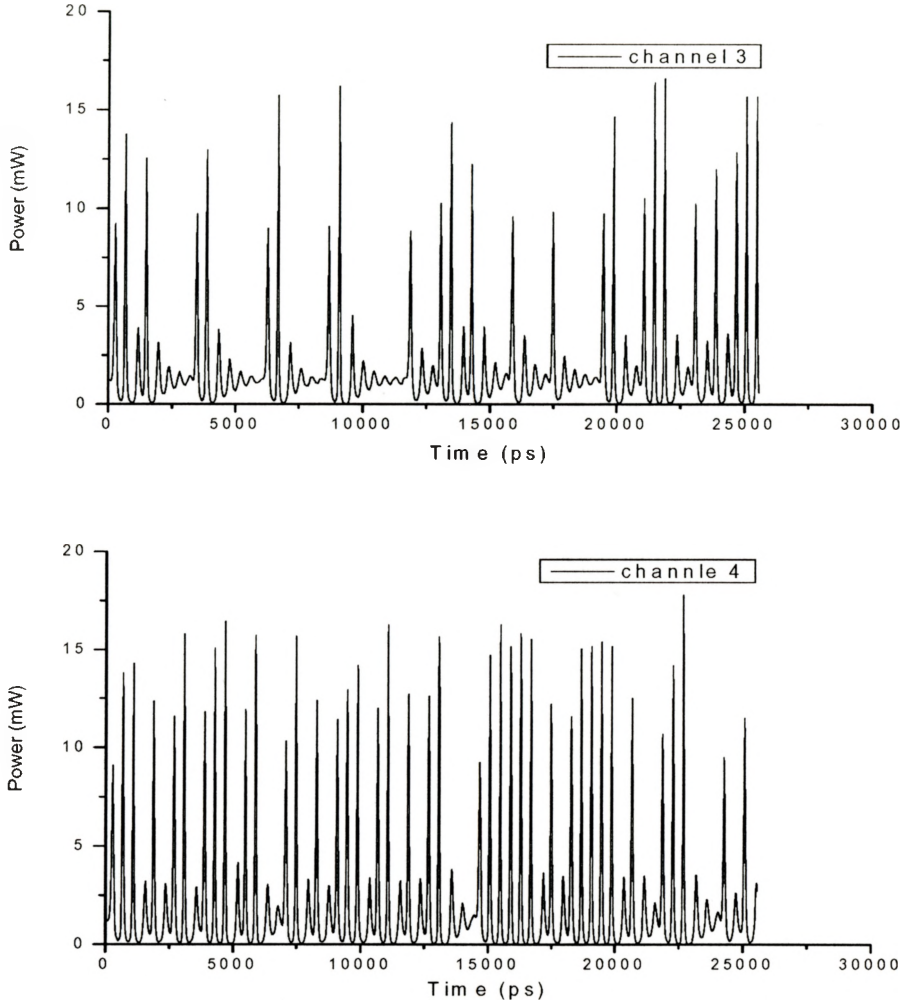

Figure 7-7 Laser output after direct modulation

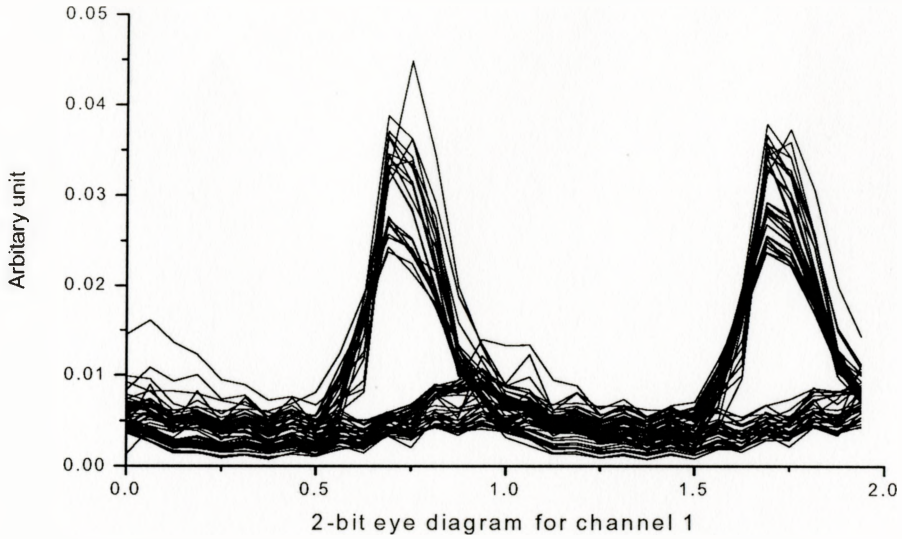
0.05
0.04
0.03
0.02
0.01
0.00
Arbitary unit
0.0
0.5
1.0
1.5
2.0
2-bit eye diagram for channel 1

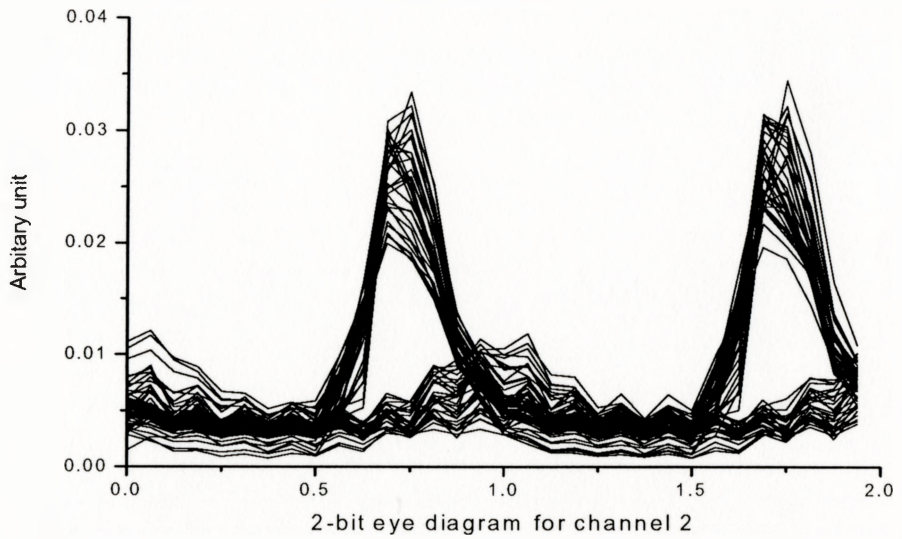
0.04
0.03
0.02
0.01
0.00
Arbitary unit
0.0
0.5
1.0
1.5
2.0
2-bit eye diagram for channel 2

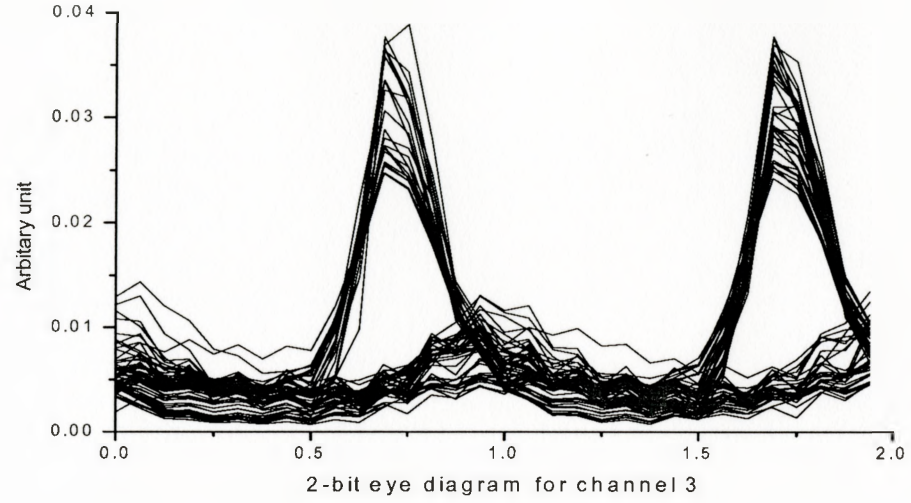

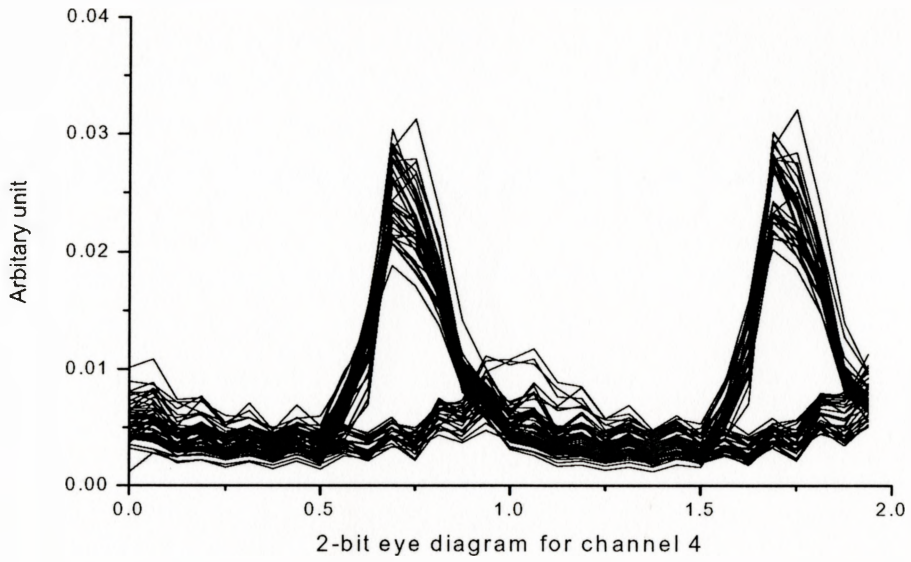

Figure 7-8 Eye diagram after fibers, EDFA and photon-detector

From all system level simulation, we can get any combinations or set any parameters according to the experiment requirement, further, getting the relatively reasonable simulation results without costing much more money and effort to set up real test project.

CONCLUSION AND FUTURE WORK

In this work, a multimode rate equation model is extracted as the governing equations for the simulation of the semiconductor laser performance. Both spontaneous emission noise and carrier shot noise have been incorporated in this model. A numerical algorithm is developed for solving these equations as analytical solutions generally don't exist. The calculated results are qualitatively compared with the experimental data and the results in literature while no discrepancy has been detected. Together with the solvers developed for other components by my colleagues, a system simulation platform is further developed on top of this laser simulator. This platform is capable of dealing with point-to-point multi-channel optical links with different configurations and parameters. As an application example, simulation results are obtained for several typical directly modulated FP lasers applied in coarse wavelength division multiplexing (CWDM) optical links running at 4×2.5Gb/s.

There are, however, still a few drawbacks in this laser model. Firstly, the symmetrical parabolic assumption over simplifies the material gain profile. Secondly, the linewidth enhancement factor is not self-consistently calculated through the refractive index change. Both of them make the material parameters inaccurate and may result in amplified inaccuracy on the laser performance. Thirdly, the non-uniform distribution of the carrier and the photon is ignored; i.e., the longitudinal spatial hole burning (LSHB) effect cannot be treated. This makes the simulation of the DFB or DBR laser not possible. Works related to solve these problems naturally become our future research topics.

APPENDIX

Devices Parameters Used in the System Simulation:

- RCG Parameters

------RCG-Pattern-Length-DATATYPE-LONG-NO-UNIT-
32
------RCG-POWER/AMPLITUDE-DATATYPE-DOUBLE-UNIT-mW/mV-
1.
------RCG-BITSHAPE-DATATYPE-{rectangle,gpulse,triangle,rcosine}-NO-UNIT-
gpulse
------RCG-VARIANCE-DATATYPE-DOUBLE-NO-UNIT-(PERCENTAGE)-
2.
------RCG-DUTY-CYCLE-DATATYPE-DOUBLE-NO-UNIT-(PERCENTAGE)-
100.
------RCG-AREA/AMPLITUDE-CONDITION-DATATYPE-DOUBLE-NO-UNIT-
amplitude

- Laser Parameters

------LD-CHOICE--1>BULK--2>QW--
1
------LD-LENGTH-UNIT-um-
300
------LD-WIDTH-UNIT-um-
2

------LD-DEPTH-UNIT-um-

0.2

------GROUP-INDEX-UNIT-NONE

3.9

------K-PETERMANN-FACTOR-

1

------POPULATION-INVERSION-FACTOR-

2

------CAVITY-LOSS-UNIT-cm-

20

------LINEWIDTH-ENHANCEMENT-FACTOR-

3

------CARRIER-LIFETIME-UNIT-1e-9s-

1.0

------PHOTON-LIFETIME-UNIT-1e-12s-

3.0

------CONFINEMENT-FACTOR-UNIT-NONE-

0.3

------GAIN-COEFFICIENT-BULK-UNIT-1e-16 *m^2-

3.0

------GAIN-COEFFICIENT-QW-UNIT-cm^-1-

1000

------GAIN-SATURATION-FACTOR-UNIT-1e-17-

2

------CARRIER-DENSITY-AT-TRANSPARENCY-UNIT-1e18*m^-3-

1.0

------GAIN-WIDTH-UNIT-nm-

49.2

------NOISE-SWITCH-
1

- Fiber Parameters:

------FIB-STEP-SIZE-UNIT-km-
60.
------FIB-ATTENUATION-UNIT--
0.10
------FIB-SECOND-ORDER-DISPERSION-UNIT--
0.
------FIB-THIRD-ORDER-DISPERSION-UNIT--
-1.117
------FIB-NON-LINEAR-GAMA-DISPERSION-UNIT--
0.
------FIB-NUMBER-OF-STEPS-UNIT--
20

- EDFA Parameters:

------EDFA-FIBER-LENGTH-UNIT-m-
100.
------EDFA-CONFINEMENT-FACTOR-UNIT-NONE-
0.505
------EDFA-PUMPING-WAVELENGTH-UNIT-nm-
1480.
------EDFA-EFFECTIVE-CORE-AREA-UNIT-e^12*m^2-
3.455752

------EDFA-FLUORESCENCE-TIME-UNIT-ms-
12.
------EDFA-PL-UNIT-NONE-
2.
------EDFA-FORWARD-PUMPING-POWER-UNIT-mW-
36.
------EDFA-BACKWARD-PUMPING-POWER-UNIT-mW-
0.
------EDFA-DOPING-CONCENTRATION-UNIT-e^23*m^-3
9.28

- Photo-detector Parameter

------FIB-RESPONSE-TIME-UNIT-ps-
200.
------FIB-GAIN-NO-UNIT-
1.
------FIB-RESPONSIVITY-UNIT-A/W-
2.

BIBLIOGRAPHY

[1] Homar, M.; Moloney, J. V.; San Miguel, M.;, " Traveling wave model of a multimode Fabry-Perot laser in free running and external cavity configurations", Quantum Electronics, IEEE Journal of, Volume: 32 Issue: 3, Page(s): 553 -566 March 1996.

[2] Ogita, S.; Lowery, A.J.; Tucker, R.S.;, "Influence of asymmetric nonlinear gain on the transient intensities of longitudinal modes in long wavelength Fabry-Perot laser diodes", Quantum Electronics, IEEE Journal of , Volume: 33 Issue: 2 , , Page(s): 198 -210 Feb. 1997

[3] Kozlowski, D.A.; Young, S.; Plumb, S.; England, J.M.C.; Time-domain modeling of mode suppression in 1.3-μm Fabry-Perot lasers, Photonics Technology Letters, IEEE , Volume: 8 Issue: 6 , , Page(s): 755 -757 June 1996

[4] Xun Li; Wei-Ping Huang; "Simulation of DFB semiconductor lasers incorporating thermal effects", Quantum Electronics, IEEE Journal of , Volume: 31 Issue: 10 , Page(s): 1848 -1855 Oct. 1995

[5] McDonald, D.; O'Dowd, R.F.;" Comparison of two- and three-level rate equations in the modeling of quantum-well lasers",Quantum Electronics, IEEE Journal of , Volume: 31 Issue: 11, Page(s): 1927 -1934, Nov. 1995

[6] Schunk, N.; Petermann, K.; "Noise analysis of injection-locked semiconductor injection lasers", Quantum Electronics, IEEE Journal of , Volume: 22 Issue: 5 Page(s): 642 -650, May 1986

[7] Ahmed,M.; Yamada,M.; Saito,M.; "Numerical modeling of intensity and phase noise in semiconductor lasers" Quantum Electronics, IEEE Journal of , Volume: 37 Issue: 12 , Page(s): 1600 -1610, Dec. 2001

[8] Wang, J.; Petermann, K.; "Noise analysis of semiconductor lasers within the coherence collapse regime", Quantum Electronics, IEEE Journal of, Volume: 27 Issue: 1: Page(s): 3 - 9, Jan. 1991

[9] D. E. McCumber, "Intensity fluctuations in the output of CW laser oscillators,"Phys. Rev., Volume: 141, Page(s): 306–322, 1966.

[10] H. Haug, "Quantum-mechanical rate equations for semiconductor lasers," Phys. Rev., Volume: 184, Page(s): 338–348, 1969.

[11] M. Lax, Rev. Mod. Phys. 38, 541 (1966); IEEE J. Quantum Electron. 3, 37 (1967).

[12] C.H. Henry, IEEE J. Quantum Electron. 18, 259,1982; 19, 1391,1983; J. Lightwave Technol. 4, 298, 1986

[13] G.P.Agrawal and N.K.Dutta, Semiconductor Lasers, 2nd ed. Van Nostrand Reinhould, New York, 1993.

[14] K.Petermann, Laser Diode Modulation and Noise, 2nd ed. Kluwer Academic, Boston, 1991.

[15] William. H. Press, Saul. A. Teukolsky, Willian. T. Vetterling, and Brian. P. Flannery,"Numerical Recipes in Fortran: The Art of Scientific Computing".Cambridge, MA: Cambridge Univ. Press, 1992.

[16] William H. Press, Brian P. Flannery, Saul A. Teukolsky, William T. Vetterling "Numerical Recipes in C Example Book : The Art of Scientific Computing" Cambridge, MA: Cambridge Univ. Press, 1993.

[17] Govind P. Agrawal, "Fiber-Optic Communication Systems", 2nd ed.; New York, John Wiley & Sons,Inc. 1997

[18] Tromborg, B.; Lassen, H.E.; Olesen, H.; "Traveling wave analysis of semiconductor lasers: modulation responses, mode stability and quantum mechanical treatment of noise spectra", Quantum Electronics, IEEE Journal of , Volume: 30 Issue: 4 Page(s): 939 -956, April 1994

[19] K. Petermann, "Calculated spontaneous emission factor for double-heterostructure injection lasers with gain-induced waveguiding", Quantum Electronics, IEEE Journal of , Volume: 15 Issue: 7 , Page(s): 566 -570, Jul 1979

[20] Agrawal, G.P.; "Effect of gain and index nonlinearities on single-mode dynamics in semiconductor lasers"Quantum Electronics, IEEE Journal of , Volume: 26 Issue: 11 , Page(s): 1901 -1909, Nov. 1990

[21] Marcenac, D.D.; Carroll, J.E.; "Modeling of intensity noise including squeezing in DFB and Fabry-Perot semiconductor laser diodes", Quantum Electronics, IEEE Journal of , Volume: 30 Issue: 9 Page(s): 2064 -2072, Sept. 1994

[22] P.S. Zory, Jr. Ed., Quantum Well Lasers, Academic Press, San Diego, CA, 1993

[23] Cartledge, J.C.; Srinivasan, R.C.; "Extraction of DFB laser rate equation parameters for system simulation purposes"Lightwave Technology, Journal of , Volume: 15 Issue: 5 Page(s): 852 -860, May 1997

[24] C. H. Henry, , "Phase noise in injection lasers," IEEE J. Lightwave Technol., vol. LT-4, Page(s): 298–311, 1986.

[25] S. Gonda and S. Mukai, "Degradation and intensity fluctuations in CW AlGaAs double-heterostructure junction lasers," IEEE J. Quantum Electron, vol. QE-11, Page(s): 545–550, 1975.